NOISE-ADAPTIVE LAYERWISE LEARNING RATES: ACCELERATING GEOMETRY-AWARE OPTIMIZATION FOR DEEP NEURAL NETWORK TRAINING

Anonymous authors
Paper under double-blind review

ABSTRACT

Geometry-aware optimization algorithms, such as Muon, have achieved remarkable success in training deep neural networks (DNNs). These methods leverage the underlying geometry of DNNs by selecting appropriate norms for different layers and updating parameters via norm-constrained linear minimization oracles (LMOs). However, even within a group of layers associated with the same norm, the local curvature can be heterogeneous across layers and vary dynamically over the course of training. For example, recent work shows that sharpness varies substantially across transformer layers and throughout training, yet standard geometry-aware optimizers impose fixed learning rates to layers within the same group, which may be inefficient for DNN training.

In this paper, we introduce a *noise-adaptive layerwise learning rate* scheme on top of geometry-aware optimization algorithms and substantially accelerate DNN training compared to methods that use fixed learning rates within each group. Our method estimates gradient variance in the dual norm induced by the chosen LMO *on the fly*, and uses it to assign time-varying noise-adaptive layerwise learning rates within each group. We provide a theoretical analysis showing that our algorithm achieves a sharp convergence rate. Empirical results on transformer architectures such as LLaMA and GPT demonstrate that our approach achieves faster convergence than state-of-the-art optimizers.

1 INTRODUCTION

Optimization algorithms are cornerstones for modern deep learning, enabling the training of increasingly large neural networks, such as LLaMA (Touvron et al., 2023) and GPT (Achiam et al., 2023) models. While standard optimizers such as SGD (Robbins & Monro, 1951) and Adam (Kingma & Ba, 2014) remain widely used, they often overlook the geometry of neural network parameter spaces. Recently, geometry-aware optimization algorithms such as Muon (Jordan et al., 2024) have demonstrated remarkable empirical success by performing orthogonalized updates on matrix parameters. Building on this idea, Pethick et al. (2025) developed a framework that selects appropriate norms for different layers and updates parameters via norm-constrained linear minimization oracles (LMOs). These methods go beyond standard optimizers by exploiting structural properties (e.g. layer-wise operator norms) of DNNs rather than treating all parameters uniformly, thus leading to improved performance and acceleration for large-scale foundation model pretraining (Liu et al., 2025).

Despite their success, most of the existing geometry-aware optimizers simply assign fixed learning rates within groups of layers associated with the same norm choice. However, these algorithms neglect the heterogeneous and dynamic nature of various layers during the neural network training. For example, recent studies (Wang et al., 2025) have shown that sharpness or local curvature of the objective function can vary substantially across different types of layers (e.g., query-key (QK) layers, value-output (VO) layers, and multilayer perceptron (MLP) in transformers). Moreover, these variations evolve over time, as observed when training with AdamW (Loshchilov & Hutter, 2017). (Riabinin et al., 2025) firstly proposed layerwise learning rates for the geometry-aware optimization methods based on smoothness parameters. In contrast, we focused on the noise magnitude of each layer instead of the smoothness parameters. In particular, we have observed similar phenomena in training a LLaMA model with the Muon optimizer[1]. Figure 1 highlights that the stochastic gradient

[1]We follow `https://github.com/KellerJordan/modded-nanogpt` to apply Muon optimizer to the transformer hidden layers (including query, key, value, output, MLP layers), and AdamW to the embedding, LM head, normalization layers.

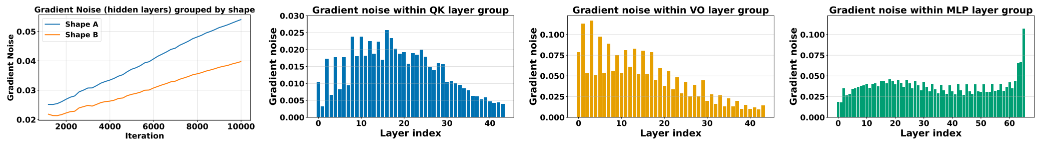

Figure 1: The stochastic gradient noise is heterogeneous across groups and layers in transformers. The first subfigure shows that average gradient noise in hidden layers varies across parameter groups defined by matrix shape and evolves over training. The last three subfigures illustrate that, within each layer group, the gradient noise varies substantially across layers[3].

noise differs substantially across layer groups or layers, and shifts throughout training. Nevertheless, state-of-the-art geometry-aware optimizers such as D-Muon (Liu et al., 2025) and Scion (Pethick et al., 2025) use the same fixed learning rate for matrices of the same shape, ignoring the fact that gradient noise on layers with the same shape can vary significantly over iterations as shown in Figure 1. This mismatch suggests that treating such layers uniformly may lead to inefficient training, motivating the need for novel layerwise learning rate schemes.
Layerwise adaptive learning rates (You et al., 2017; 2019) are widely used in deep learning under standard Euclidean spaces. These optimizers automatically rescale updates according to gradient magnitudes, which reduces manual tuning and often accelerates convergence. However, they disregard the structural geometry of neural networks by treating all parameters as if they belonged to the same category. In reality, neural networks contain diverse parameter groups such as matrices in attention layers, vectors in bias terms, and embedding tables, where different layers in each group exhibit vastly different noise profiles as illustrated in our Figure 1. The key open question is how to design adaptive learning rates beyond standard Euclidean spaces, enabling geometry-aware optimizers to exploit heterogeneous gradient noise across layers and over the course of training.

In this paper, we propose a new geometry-aware optimization algorithm named *Lanton: LAyer-wise Noise-adaptive learning raTe scaling with Operator Norms*. Our algorithm dynamically estimates gradient variance in the dual norm induced by the chosen LMO and uses this estimate to assign layerwise learning rates that adapt over the course of training. Unlike existing approaches, which treat all layers in a group uniformly, our algorithm accounts for the heterogeneity of gradient noise across layers, leading to smaller learning rates for layers with larger gradient noise, thereby enabling finer-grained and more efficient optimization. Importantly, the proposed mechanism is compatible with the geometry-aware optimizers, such as Muon (Jordan et al., 2024) and D-Muon (Liu et al., 2025). Our contribution can be summarized as follows.

- We propose a new optimization algorithm named *LANTON: LAyer-wise Noise-adaptive learning raTe scaling with Operator Norms*, which can dynamically capture the gradient noise of each layer and thus accordingly rescale the learning rate of each layer.
- We prove that our method achieves a sharp convergence rate of $\tilde{O}(1/\sqrt{T}+\sqrt{\sum_\ell \bar{\sigma}_\ell}/T^{1/4})$, where $\bar{\sigma}_\ell$ denotes an upper bound on the gradient noise of the layer ℓ. Our bound shows improved noise dependence under the layer-wise noise assumption. By explicitly accounting for the heterogeneous noise levels across layers, our analysis demonstrates the advantage of noise-adaptive layer-wise learning rates.
- Empirically, we evaluate our approach on language model training and image classification, including LLaMA, GPT2 and convolutional neural network, and show that it substantially accelerates training and improves sample efficiency compared to state-of-the-art optimizers. Our results indicate that dynamically adapting learning rates at the layer level can better capture the evolving optimization landscape, leading to faster convergence and improved training efficiency. Together, these contributions highlight the importance of integrating noise adaptivity into geometry-aware optimization and open new directions for scalable and effective training of deep neural networks.

2 Related Work

A long line of work has studied optimization for deep learning. The most classical method is SGD (Robbins & Monro, 1951). Early advances focused on adaptive learning rates, including Adagrad

[3]See Appendix F for the implementation details.

(Duchi et al., 2011), RMSProp (Tieleman & Hinton, 2012), Adadelta (Zeiler, 2012), and the widely used Adam (Kingma & Ba, 2014). Later developments improved Adam in various ways: AdamW (Loshchilov & Hutter, 2017) introduced decoupled weight decay and has become the default choice for deep learning; several variants incorporate variance reduction, such as AdEMAMix (Pagliardini et al., 2024) and MARS-AdamW (Yuan et al., 2024); others target memory efficiency, including Adafactor (Shazeer & Stern, 2018), Lion (Chen et al., 2023), MeZO (Malladi et al., 2023), GaLore (Zhao et al., 2024a), Adam-mini (Zhang et al., 2024), and Signum (Zhao et al., 2024b).

Another line of work approximates or leverages second-order information. K-FAC (Martens & Grosse, 2015) and Shampoo (Gupta et al., 2018) are classical examples. The substantial compute and memory overheads of second-order optimizers have motivated distributed implementations of Shampoo (Anil et al., 2020; Shi et al., 2023). More recently, lightweight preconditioned optimizers such as Sophia (Liu et al., 2023a) and SOAP (Vyas et al., 2024) have been proposed, achieving substantial speedups over AdamW in large-scale language model pretraining.

A third research direction focuses on layer-wise or block-wise learning rates to accelerate training. LARS (You et al., 2017) and LAMB (You et al., 2019) are widely used for large-batch training, while more recent approaches extend AdamW with blockwise learning rates (Wang et al., 2025).

Several parameter-free or schedule-free optimizers aim to reduce the burden of hyperparameter tuning, including Dog (Ivgi et al., 2023), Prodigy (Mishchenko & Defazio, 2023), and Schedule-Free AdamW (Defazio et al., 2024).

Most recently, the theory of modular duality in optimization and the perspective of steepest descent under different operator norms (Bernstein & Newhouse, 2024a;b; Large et al., 2024) have inspired the design of matrix-based and geometry-aware optimizers, including Muon (Jordan et al., 2024) and Scion (Pethick et al., 2025), as well as distributed implementations such as D-Muon (Liu et al., 2025) and Dion (Ahn et al., 2025), which further improve training efficiency and stability at scale.

3 Preliminaries

In this work, we consider the stochastic optimization problem $\min_X f(X) := \mathbb{E}_{\xi\in\mathcal{D}}[F(X;\xi)]$, where ξ is random noise sampled from an unknown distribution $\mathcal{D}$, and $X \in \mathcal{S}$ is the model parameter, where $X = [X_1, \ldots, X_p]$, $X_i \in \mathcal{S}_i := \mathbb{R}^{m_i\times n_i}$, and $\mathcal{S} := \bigotimes_{i=1}^p \mathcal{S}_i$. Similarly, write the gradient as $\nabla f(X) = [\nabla_1 f(X), \ldots, \nabla_p f(X)] \in \mathcal{S}$, and the stochastic gradient as $\nabla F(X;\xi) = [\nabla_1 F(X;\xi), \ldots, \nabla_p F(X;\xi)] \in \mathcal{S}$ (here we adopt the notation and setup from (Riabinin et al., 2025). We assume that the objective is bounded from below, i.e., $f^* := \inf_X f(X) > -\infty$.

Notations. Let $\|\cdot\|$ denote an arbitrary (not necessarily Euclidean) vector/matrix norm with associated dual norm $\|\cdot\|_*$, and let $\|\cdot\|_{\text{nuc}}$ denote the nuclear norm. We use $\langle\cdot,\cdot\rangle$ for the trace inner product, defined as $\langle A, B\rangle = \text{tr}(A^\top B)$ for $A, B \in \mathbb{R}^{m\times n}$. For two positive functions f and g, we write $f \lesssim g$ (resp. $f \gtrsim g$) if there exists $c > 0$ such that $f(x) \le cg(x)$ (resp. $f(x) \ge cg(x)$) for all x. We use standard big-O notation, with $\tilde{O}$ and $\tilde{\Omega}$ used to hide polylogarithmic factors, respectively.

Linear Minimization Oracle (LMO). The LMO is a fundamental concept in convex optimization (Frank et al., 1956), particularly in the context of algorithms like the Frank-Wolfe algorithm (also known as the conditional gradient method (Jaggi, 2013)). Given a convex feasible set $\mathcal{K}$ and a direction vector/matrix u, the LMO returns an extreme point of $\mathcal{K}$ that minimizes the linear function $\langle u, x\rangle$ over $\mathcal{K}$. Mathematically, this can be expressed as: $\text{LMO}(u) = \arg\min_{x\in\mathcal{K}}\langle u, x\rangle$.

Throughout this paper, we focus on the special case where $\mathcal{K} := \{x \mid \|x\| \le 1\}$ for some chosen (not necessarily Euclidean) norm $\|\cdot\|$ (Pethick et al., 2025), unless specified otherwise.

Operator Norm and RMS Norm. Given a matrix $A \in \mathbb{R}^{m\times n}$ and two normed vector spaces $(\mathbb{R}^n, \|\cdot\|_a)$ and $(\mathbb{R}^m, \|\cdot\|_b)$, the "$a$ to b" induced operator norm is defined as $\|A\|_{a\to b} := \max_{x\in\mathbb{R}^n, x\neq 0} \frac{\|Ax\|_b}{\|x\|_a} = \sup_{\|x\|_a=1}\|Ax\|_b$. Given a vector $x \in \mathbb{R}^d$, the RMS norm is defined as $\|x\|_{\text{RMS}} := \frac{1}{\sqrt{d}}\|x\|_2$.

4 Our Method

Algorithmic Framework. Our proposed algorithmic framework (Algorithm 1) consists of three main stages at each iteration. First (lines 4-6), we compute the stochastic gradient G_t^ℓ for each layer,

Algorithm 1 LANTON: LAyer-wise Noise-adaptive raTe scaling with Operator Norms

```
1: Input: $X_0, \alpha, \beta_1, \beta_2, \gamma, \eta, G_0 = \nabla F(X_0; \xi_0), B_0 = G_0$
2: while $t < T$ do
3:   for each layer $\ell$ do
4:     $G_t^\ell = \nabla_\ell F(X_t; \xi_t)$, $\tilde{G}_t^\ell = \nabla_\ell F(X_t; \tilde{\xi}_t)$        ($\tilde{G}_t^\ell$ is used only in Option II)
5:     $B_t^\ell = \beta_1 B_{t-1}^\ell + (1-\beta_1) G_t^\ell$
6:     $O_t^\ell = \mathrm{LMO}(B_t^\ell)$        (choose norm based on $\ell$'s group $\mathcal{G}_\ell$, Table 1 line 5)
7:     $H_t^\ell = \beta_2 H_{t-1}^\ell + (1-\beta_2) \cdot \begin{cases} \|G_t^\ell - G_{t-1}^\ell\|_*^2 & \text{Option I (practical)} \\ \|G_t^\ell - \tilde{G}_t^\ell\|_*^2 & \text{Option II (theoretical)} \end{cases}$        (Table 1 line 4)
8:     $\alpha_t^\ell = \alpha / \sqrt{\alpha^2 + H_t^\ell}$, $\alpha_t^m = \max_{\ell \in \mathcal{G}_\ell} \alpha_t^\ell$        (max is over $\ell$'s group $\mathcal{G}_\ell$, Table 1 line 1)
9:     $\eta_t^\ell = \eta_t \sqrt{\alpha_t^\ell / \alpha_t^m}$        ($\eta_t \in [\eta_{\min}, \eta_{\max}]$ follows a cosine decay schedule)
10:    $X_{t+1}^\ell = X_t^\ell - \eta_t^\ell O_t^\ell$
11:  end for
12: end while
```

Table 1: The choice of LMO can be different between layers. We use $W \in \mathbb{R}^{d_{\text{out}} \times d_{\text{in}}}$ to denote a matrix and $w \in \mathbb{R}^d$ to denote a vector. Write the SVD as $W = U\Sigma V^\top$.

Parameter Group	Hidden layers (query, key, value, output, mlp)	Embedding, LM head layers	RMS norm
Size	Matrix $\in \mathbb{R}^{d_{\text{out}} \times d_{\text{in}}}$	Matrix $\in \mathbb{R}^{d_{\text{out}} \times d_{\text{in}}}$	Vector $\in \mathbb{R}^d$
Norm $\|\cdot\|$	RMS $\to$ RMS	$1 \to \infty$	RMS
Dual Norm $\|\cdot\|_*$	$\sqrt{d_{\text{out}}/d_{\text{in}}}\|\cdot\|_{\text{nuc}}$	$\|\cdot\|_{1\to1}$	$\sqrt{d}\|\cdot\|_2$
LMO	$-\sqrt{d_{\text{out}}/d_{\text{in}}}UV^\top$	$-\frac{1}{d_{\text{in}}}\,\mathrm{sign}(W)$	$-\sqrt{d}\frac{w}{\|w\|_2}$
LMO Implementation	Newton-Schulz	Signum	RMS Normalization

accumulate its momentum B_t^ℓ, and then obtain the direction $O_t^\ell = \mathrm{LMO}(B_t^\ell)$ by invoking a LMO, where the choice of norm depends on the structural group of layer ℓ (embedding/LM head layers, hidden layers, or non-matrix layers; see Table 1). Note that line 4-6 is the same as the work of Scion (Pethick et al., 2025) and Gluon (Riabinin et al., 2025). Second (lines 7-9), the key novelty of our framework is to incorporate noise-adaptive layer-wise learning rate scaling. We maintain a momentum buffer H_t^ℓ to track the moving average of the estimated noise level for each layer. This buffer can be updated in two ways: a practical option (using G_t^ℓ and G_{t-1}^ℓ and avoiding extra computation) and a theoretical option (using two independent stochastic gradients G_t^ℓ and $\tilde{G}_t^\ell$ at each step). Based on H_t^ℓ, the layer-wise scaling α_t^ℓ is computed, and the effective learning rate is adjusted proportionally through the ratio α_t^ℓ/α_t^m, ensuring that layers with larger noise magnitudes employ smaller learning rates. Finally (lines 10-11), we update the model parameters with the scaled stepsize and the direction given by LMO.

Choice of Norm Constraint and LMO Implementation. To determine appropriate norm constraints for different types of parameters in deep neural networks, we adopt the operator norm perspective recently advanced in (Large et al., 2024; Bernstein & Newhouse, 2024a; Pethick et al., 2025). As summarized in Table 1, parameters naturally fall into three groups: (i) hidden layers (e.g., query, key, value, output, and MLP weights), which are represented as matrices and we use the RMS $\to$ RMS operator norm with dual nuclear norm (scaled by $\sqrt{d_{\text{out}}/d_{\text{in}}}$); (ii) weight-sharing layers such as embedding and LM head matrices, where the $\ell_1 \to \ell_\infty$ operator norm is used with dual $\ell_1 \to \ell_1$ norm; and (iii) non-matrix parameters like RMS normalization vectors, where the RMS norm with dual ℓ_2 norm (scaled by $\sqrt{d_{\text{model}}}$) is adopted. These dual norms are critical in line 7 of Algorithm 1 for estimating the layer-wise gradient noise magnitude. Based on the chosen norms, the corresponding LMOs in line 6 of Algorithm 1 also differ across parameter types: for hidden layers, the LMO corresponds to a scaled $UV^\top$ computed efficiently via Newton-Schulz iterations; for embedding and LM head layers, the LMO reduces to a scaled element-wise sign operator; and for RMS normalization vectors, the LMO is implemented by RMS normalization. This unified design of norm constraints, dual norms, and LMOs with their implementations ensures both theoretical consistency with our algorithmic framework and practical efficiency in large-scale deep learning.

Noise-Adaptive Layer-wise Learning Rates. To capture the heterogeneous noise levels across different layers, we introduce noise-adaptive layer-wise learning rates, which dynamically scale the stepsize of each layer according to its estimated stochastic gradient variance. Specifically, we maintain a variance tracker $H_t^\ell = \beta_2 H_{t-1}^\ell + (1-\beta_2)\|G_t^\ell - \tilde{G}_t^\ell\|_*^2$ (line 7), where $\beta_2 \in (0,1)$ serves as a momentum-like parameter that smooths the estimate, akin to second-moment accumulation in adaptive optimizers. The resulting adaptive scaling factor $\alpha_t^\ell = \alpha/\sqrt{\alpha^2 + H_t^\ell}$ (line 8) ensures that layers subject to higher noise levels (large H_t^ℓ) receive proportionally smaller effective learning rates, consistent with classical stochastic optimization theory. We implement this by reweighting the base learning rate with the ratio α_t^ℓ/α_t^m (where $\alpha_t^m = \max_{\ell \in \mathcal{G}_\ell} \alpha_t^\ell$), thereby aligning the updates across layers under a unified theoretical principle. While our theoretical framework (see Section 5) assumes two independent gradient estimates G_t^ℓ and $\tilde{G}_t^\ell$, in practice we approximate $\tilde{G}_t^\ell$ by the previous step gradient G_{t-1}^ℓ. This avoids doubling the batch size and keeps the total number of sampled data consistent with standard baselines, thus ensuring fair comparisons in empirical evaluation.

Comparison with Other Optimizers. Compared to Muon (Jordan et al., 2024), Scion (Pethick et al., 2025), Gloun (Riabinin et al., 2025), and D-Muon (Liu et al., 2025), our method introduces noise-adaptive layer-wise learning rates by estimating gradient variance in the dual norm induced by the chosen LMO. Unlike Muon and D-Muon, which use AdamW for embedding and LM head layers, we adopt a geometry-aware framework (similar to Scion) and update these weight-sharing layers with Signum (see Table 1).

Optimizers such as LARS (You et al., 2017) and LAMB (You et al., 2019) also use layer-wise rescaling to stabilize large-batch training. However, these methods treat all layers uniformly. In contrast, our algorithm is geometry-aware, selecting norms tailored to hidden, embedding, and normalization layers, and updating them through LMOs with noise-adaptive scaling.

Finally, although Algorithm 1 resembles Gong et al. (2025) in estimating noise magnitude, there are key differences. Our method is LMO-based and works under arbitrary norms, while Gong et al. (2025) is restricted to the Euclidean space. Our noise adaptivity refers to per-layer scaling based on estimated variance, whereas theirs targets convergence without prior noise knowledge. Moreover, our moving-average variance estimator H_t^ℓ remains $O(1)$ with high probability, in contrast to their cumulative estimator $\sum_{k=1}^t \|G_k - \tilde{G}_k\|^2$ which grows as $O(\sqrt{t})$.

5 Analysis

In this section, we provide theoretical convergence guarantees for Algorithm 1. Let $\|\cdot\|_{(\ell)}$ denote the chosen norm of layer ℓ with dual norm $\|\cdot\|_{(\ell)*}$, and let p be the number of layers. We begin by presenting the assumption of layer-wise L-smoothness. Importantly, we do not assume that either the primal norm $\|\cdot\|_{(\ell)}$ or the dual norm $\|\cdot\|_{(\ell)*}$ is Euclidean. A similar layer-wise smoothness assumption is also imposed in Riabinin et al. (2025) to capture the geometry of neural networks.

Assumption 5.1. The objective f is layer-wise L-smooth with constants $L := (L_1, \dots, L_p) \in \mathbb{R}_+^p$, i.e., for all $\ell = 1, \dots, p$, $X = [X_1, \dots, X_p]$, and $Y = [Y_1, \dots, Y_p]$, $\|\nabla_\ell f(X) - \nabla_\ell f(Y)\|_{(\ell)*} \leq L_\ell \|X_\ell - Y_\ell\|_{(\ell)}$.

Our second assumption states that the stochastic gradient oracle is unbiased and the layer-wise gradient noise is almost surely bounded both above and below in the dual space.

Assumption 5.2. (i) The stochastic gradient oracle is unbiased, i.e., $\mathbb{E}[\nabla F(X,\xi) \mid X] = \nabla f(X)$. (ii) It holds with probability one for all ℓ that $\underline{\sigma}_\ell \leq \|\nabla_\ell F(X,\xi) - \nabla_\ell f(X)\|_{(\ell)*} \leq \bar{\sigma}_\ell$ with $\underline{\sigma}_\ell \geq 0$.

Compared to the standard bounded variance assumption (used for expectation-based analysis) or the almost surely bounded-noise assumption (used for high-probability analysis) in stochastic optimization, Assumption 5.2 additionally requires that the stochastic gradient noise is almost surely lower bounded. A similar assumption is also made in (Gong et al., 2025). In the noisy setting, we assume $0 < \underline{\sigma}_\ell \leq \bar{\sigma}_\ell$, while in the noiseless setting we have $\bar{\sigma}_\ell = \underline{\sigma}_\ell = 0$. Note that in practice, we are always in the noisy setting where $0 < \underline{\sigma}_\ell \leq \bar{\sigma}_\ell$, as illustrated in Figure 1. From a technical perspective, this assumption is crucial for establishing a tight lower bound on α_t^ℓ/α_t^m. For further proof details, see Lemma 5.5.

We now present our main result. Here C_1, C_2 (with $C_2 \geq 1$) are the universal constants defined in Lemma A.3, which may depend on the dimension of the model parameters. Depending on the choice of norm constraint, one may select different C_1, C_2 to obtain tighter dimension-dependent bounds, rather than applying a uniform choice. A detailed discussion is provided in Remark A.4.

Theorem 5.3. *Suppose Assumptions 5.1 and 5.2 hold. Let* $\Delta_1 = f(X_1) - f^*$. *Set* $\beta_1 = 1 - \alpha$ *with* $\alpha = \min\left(\frac{\sqrt{\Delta_1 \sum_\ell L_\ell}}{\sum_\ell \bar{\sigma}_\ell \sqrt{T}}, 1\right)$, $1 - \min_\ell \frac{\sigma_\ell^4}{32(2C_2\bar{\sigma}_\ell^2 - \sigma_\ell^2)^2 \log(4T/\delta)} \leq \beta_2 < 1$, $\eta_{\max} = \sqrt{\frac{\Delta_1 \alpha}{\sum_\ell L_\ell T}}$, *and* $\eta_{\min} = \eta_{\max}/\kappa_\eta$ *with* $1 \leq \kappa_\eta \leq O(1)$. *With probability at least* $1-\delta$, *we have*

$$\frac{1}{T}\sum_{t=1}^{T}\sum_{\ell=1}^{p}\|\nabla_\ell f(X_t)\|_{(\ell)*} \lesssim \frac{\sqrt{C_2}(\sum_\ell \bar{\sigma}_\ell)^2}{\sqrt{\Delta_1 \sum_\ell L_\ell T}} + \frac{C_2^{3/2}}{C_1}\sqrt{\log\frac{T}{\delta}}\left(\frac{\sqrt{\Delta_1 \sum_\ell L_\ell}}{\sqrt{T}} + \frac{\sqrt{\sum_\ell \bar{\sigma}_\ell}(\Delta_1 \sum_\ell L_\ell)^{1/4}}{T^{1/4}}\right).$$

Theorem 5.3 shows that Algorithm 1 achieves a convergence rate of $\tilde{O}(1/\sqrt{T} + \sqrt{\sum_\ell \bar{\sigma}_\ell}/T^{1/4})$. Our bound highlights the advantage of adopting a layer-wise noise assumption. It achieves improved noise dependence compared to the $O(1/T^{3/4} + \sum_\ell \bar{\sigma}_{\max}/T^{1/4})$[4] bound established in (Pethick et al., 2025, Theorem 5.7), where $\bar{\sigma}_{\max}$ is the uniform noise bound assumed in prior work (Pethick et al., 2025). This improvement arises from recognizing that different layers exhibit distinct noise levels during training, and thus should not be treated uniformly. Empirically, we observe noise heterogeneity across layer groups (see Figure 1 and Table 3). Moreover, we compute that $\sqrt{\sum_\ell \bar{\sigma}_\ell} = 3.654$, which is significantly smaller than $\sum_\ell \bar{\sigma}_{\max} = 18.018$ in the LLaMA-1.1B pretraining on C4 dataset (Dodge et al., 2021), thereby validating our theoretical gain in both analysis and experiments.

5.1 Proof Outline

Here we give an outline of the proof of Theorem 5.3, containing the main components of our analysis; see Appendices B and C for full details. The proof sketch below is based on the setting of Theorem 5.3. To start, we introduce a few key definitions (with the convention $0/0 := 1$):

$$\kappa_\sigma^\ell = \begin{cases} \bar{\sigma}_\ell/\sigma_\ell & \sigma_\ell > 0 \\ 1 & \bar{\sigma}_\ell = 0 \end{cases}, \quad \kappa_\sigma = \max_\ell \kappa_\sigma^\ell, \quad \bar{\sigma}_{\max} = \max_\ell \bar{\sigma}_\ell, \quad \text{and} \quad t_0 = \frac{\log 2}{\log(1/\beta_2)}. \tag{1}$$

The following lemma provides high-probability two-sided bounds for the variance tracker H_t^ℓ, which in turn allow us to derive tight upper and lower bounds for α_t^ℓ (numerator of the noise ratio term). The key to the analysis is an application of the Azuma-Hoeffding inequality (see Lemma A.1).

Lemma 5.4. *With probability at least* $1-\delta$, *for all* ℓ *and* $t_0 \leq t \leq T$, $\frac{\sigma_\ell^2(1-\beta_2^t)}{C_2} \leq H_t^\ell \leq 4\bar{\sigma}_\ell^2(1-\beta_2^t)$.

With Lemma 5.4, we can effectively lower bound the noise ratio term α_t^ℓ/α_t^m, which is used to assign layerwise learning rates in line 9 of Algorithm 1, with high probability. Our next lemma shows that α_t^ℓ/α_t^m is both upper and lower bounded throughout training under our assumptions. Consequently, the learning rate η_t^ℓ is bounded on both sides with high probability.

Lemma 5.5. *With probability at least* $1-\delta$, *for all* ℓ *and* $t \leq T$,

$$\min\left\{\frac{\alpha}{\sqrt{\alpha^2 + 4\bar{\sigma}_{\max}^2}}, \frac{1}{2\sqrt{C_2}\kappa_\sigma}\right\} =: \alpha_r \leq \frac{\alpha_t^\ell}{\alpha_t^m} \leq 1, \tag{2}$$

and therefore, with probability at least $1-\delta$, *we have* $\alpha_r \eta_{\min} \leq \eta_t^\ell \leq \eta_{\max}$ *for all* ℓ *and* $t \leq T$.

We now provide a high-level proof sketch of our main result. See Appendix C for full proof details.

Proof sketch of Theorem 5.3. The main novelty in the proof is to leverage the magnitude of H_t^ℓ (Lemma 5.4) as a surrogate for the true stochastic gradient variance, ensuring that the noise-adaptive layerwise learning rate α_t^ℓ has roughly the same magnitude as if the stochastic gradient noise were known (Lemma 5.5). The rest of the proof proceeds similarly to that of (Cutkosky & Mehta, 2020, Theorem 1) and (Li & Hong, 2025; Shen et al., 2025; Riabinin et al., 2025). Define $\hat{\epsilon}_t^\ell = B_t^\ell - \nabla_\ell f(X_t)$ and $\epsilon_t^\ell = G_t^\ell - \nabla_\ell f(X_t)$. We begin by applying Lemma 5.5 to the descent lemma (see Lemma C.1), rearranging to obtain:

$$\sum_{t=1}^{T}\sum_{\ell=1}^{p}\eta_t^\ell\|\nabla_\ell f(X_t)\|_{(\ell)*} \leq \frac{\Delta_1}{\alpha_r\eta_{\min}} + \sum_{\ell=1}^{p}\left(\frac{2\eta_{\max}}{\alpha_r\eta_{\min}}\sum_{t=1}^{T}\|\hat{\epsilon}_t^\ell\| + \frac{\eta_{\max}^2}{2\alpha_r\eta_{\min}}L_\ell T\right).$$

[4]This rate is obtained by replacing the global variance in (Pethick et al., 2025) with the layer-wise variance.

Using L-smoothness (Assumption 5.1) and standard calculations, we have

$$\|\hat{\epsilon}_{t+1}^{\ell}\|_{(\ell)*} \leq \beta_1^t \|\hat{\epsilon}_1^{\ell}\|_{(\ell)*} + (1-\beta_1) \left\| \sum_{\tau=0}^{t-1} \beta_1^{\tau} \epsilon_{t-\tau}^{\ell} \right\|_{(\ell)*} + \eta_{\max} L_{\ell} \sum_{\tau=0}^{t-1} \beta_1^{\tau}. \tag{3}$$

Next, we apply the concentration inequality introduced in (Liu et al., 2023b, Lemma 2.4) to bound $\| \sum_{\tau=0}^{t-1} \beta_1^{\tau} \epsilon_{t-\tau}^{\ell} \|_F$, and then use the equivalence of norms (see Lemma A.3) to derive that, with probability at least $1-\delta$,

$$\left\| \sum_{\tau=0}^{t-1} \beta_1^{\tau} \epsilon_{t-\tau}^{\ell} \right\|_{(\ell)*} \leq \frac{1}{C_1} \left\| \sum_{\tau=0}^{t-1} \beta_1^{\tau} \epsilon_{t-\tau}^{\ell} \right\|_F \leq \frac{4C_2\bar{\sigma}}{C_1} \sqrt{\frac{\log(2T/\delta)}{1-\beta_1}}. \tag{4}$$

Substituting Equation (4) back into Equation (3) gives the bound for $\|\hat{\epsilon}_t^{\ell}\|_{(\ell)*}$. With suitable parameter choices as specified in Theorem 5.3, this concludes the proof. □

6 Experiments

In this section, we present the empirical results in comparison with the state-of-the-art optimizers by pretraining two mainstream transformer architectures GPT (Radford et al., 2019) and LLaMA (Touvron et al., 2023) series. The experiment of image classification is deferred to Appendix D. We include the analysis of running time in Appendix J, the ablation studies about batch size in Appendix L, the estimation method of gradient noise in Appendix M. All experiments were run on $4\times$ NVIDIA H200 graphic cards with Intel XEON Platinum 8558 CPU.

6.1 Experimental Settings

Baselines We compare our LANTON with AdamW (Loshchilov & Hutter, 2017), Muon (Jordan et al., 2024), MARS (short for MARS-AdamW) (Yuan et al., 2024), SCION (Pethick et al., 2025), D-Muon (Liu et al., 2025), the layer-wise learning rate algorithm LAMB (You et al., 2019), and block-wise learning rate algorithm BW-AdamW (Wang et al., 2025). SCION and D-Muon apply the Muon optimizer to matrix parameters in hidden layers (e.g., query, key, value, mlp), and all these algorithms use Newton-Schulz iteration (Bernstein & Newhouse, 2024b) to approximately orthogonalize the update matrix, i.e., $UV^{\top}$ in Table 1.

Models We evaluate on both GPT and LLaMA-style decoders. For GPT we use the HuggingFace GPT2 family: GPT2-small (124M parameters) and GPT2-medium (355M parameters). For LLaMA we configure two sizes: LLaMA-0.5B and LLaMA-1.1B. Unless noted, all models are decoder-only with rotary positional embeddings and RMSNorm/LayerNorm per architecture defaults. Refer to Table 4 for detailed model configuration.

Datasets We pretrain GPT2 and LLaMA models on three datasets. OpenWebText-100k is used for GPT-small/medium models, and it is a subset of Openwebtext dataset (Gokaslan et al., 2019). As there is no validation set in OpenWebText-100k, we split $90\%/10\%$ into training/validation set and train models with teacher forcing. MiniPile (Kaddour, 2023) is used for LLaMA-0.5B, where minipile is a subset of the deduplicated Pile corpus (Gao et al., 2020). C4 (Colossal Clean Crawled Corpus) (Dodge et al., 2021) is a large-scale English text corpus constructed by aggressively cleaning Common Crawl webpages, and we use it to pretrain LLaMA-1.1B following the standard text-to-token pipeline. All corpora are tokenized with the model's native tokenizer.

6.2 Training Setup and Results

6.2.1 Implementation of LANTON

We implement LANTON on top of the D-Muon (Liu et al., 2025), which carefully adjusts the update magnitudes between hidden layers and non-hidden layers (embedding and LM head layers). Let η_t denote the base learning rate at iteration t, which is compatible with annealing techniques (e.g., cosine decay). For layer ℓ, D-Muon updates the non-hidden layers using AdamW with learning rate η_t, and the hidden layers parameters $W_{\ell} \in \mathbb{R}^{d_{\text{out}}^{\ell} \times d_{\text{in}}^{\ell}}$ (i.e., QK, VO, MLP) with a rescaled learning rate $0.2\eta_t\sqrt{\max(d_{\text{in}}^{\ell}, d_{\text{out}}^{\ell})}$. LANTON further rescales the hidden-layer learning rate to

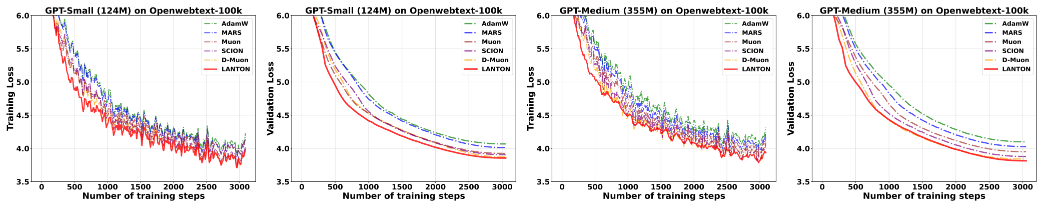

Figure 2: Training/validation loss on Openwebtext-100k datasets.

$0.2\eta_t\sqrt{\max(d^\ell_{\text{in}}, d^\ell_{\text{out}})\,\alpha^\ell_t/\alpha^m_t}$, where $\alpha^m_t = \max_{\ell\in\mathcal{G}_\ell}\alpha^\ell_t$ and $\mathcal{G}_\ell$ denotes the group of layer ℓ. This is the practical instantiation of line 9 in Algorithm 1. In our implementation, there are three layer groups, i.e., {QK, VO, MLP}, {Embedding, LM-Head}, {LayerNorm}, so there are three noise factors α^m_t accordingly. For the first layer group (hidden layers), LANTON applies Newton-Schultz iterations with 5 steps (Jordan et al., 2024) to approximate the LMO update for matrix layers. For embedding and LM head layers, LANTON uses Signum (signed momentum) with a scaled base learning rate $r_1\,\eta_t$. For LayerNorm (vector) parameters, LANTON applies RMS-normalized updates with a scaled base learning rate $r_2\,\eta_t$. Similar to SCION, which requires two distinct update scales for layer groups, LANTON also specifies two update scales r_1 and r_2, with a base learning rate η_t.

6.2.2 GPT2 on Openwebtext

We begin with small-scale experiments by pretraining GPT2 from scratch on OpenWebText-100k. All baselines (AdamW, MARS, Muon, SCION, D-Muon), and our method LANTON are trained for a single epoch with context length 512 and batch size 16. Unless otherwise specified, for all methods, we fix the random seed to 42 and weight decay parameter $\gamma = 0.1$. We apply a cosine learning-rate schedule to the base step size $\eta_{\max}$ with a linear warmup of 300 steps. After warmup, the per-step learning rate is $\eta_t = \eta_{\text{min}} + 1/2(\eta_{\text{max}} - \eta_{\text{min}})(1 + \cos(\frac{t\pi}{T}))$, where t is the step index, T is the number of training steps, and by default $\eta_{\text{min}} = 0$. The detailed hyperparameter settings for every algorithm are summarized in 5 and Table 6 in Appendix H.

As shown in Figure 2, LANTON consistently dominates all baselines (AdamW, MARS, Muon, SCION, D-Muon). Its training loss drops fastest from the earliest iterations and stays below competing methods across the entire training, indicating superior convergence speed. LANTON also achieves the lowest validation loss, exhibit superior performance.

6.2.3 LLaMA on C4 and MiniPile

We assess large-scale training by pretraining a LLaMA-1.1B model on C4 and a LLaMA-0.5B model on MiniPile with a total budget of 20B training tokens. We use the pretrained LLaMA tokenizer and set the sequence length to 256 on C4 and 512 on MiniPile. The batch size is 1024 for C4 and 300 for MiniPile. We employ a cosine learning rate schedule with a uniform warmup of 1,000 steps for all methods. Full hyperparameter settings for every baseline are reported in Tables 7 and 8 in Appendix H.

On C4, LANTON exhibits a significantly steeper loss descent in the early phase and maintains a consistent lead throughout training, while ultimately reaching validation losses comparable to other baselines (see Figure 3). We track the averaged effective learning rates within each layer group and provide the explanations for training acceleration of LANTON in Appendix K. On Minipile, although LANTON does not exhibit the lowest loss in the middle of training, it achieves the best final training loss and maintains consistently strong validation performance.

6.3 Comparison with Algorithms Using Layer-wise/Block-wise Learning Rates

To highlight the benefit of our noise-adaptive layer-wise learning rate schedule, we compare with LAMB (You et al., 2019) and the recent block-wise scheme BW-AdamW (Wang et al., 2025). LAMB modifies Adam by applying a per-layer "trust ratio" to rescale the base learning rate in each layer. BW-AdamW manually tunes the best block-specific update ratio for each parameter block. Following the original best tuned ratio, we use $r(\text{Emb}) = 10, r(\text{QK}) = 8, r(\text{VO}) = 4, r(\text{MLP/LM-Head}) = 6, r(\text{Layer norm}) = 1$ in the experiment. The compared training and validation curves are presented in Figure 4(a). LANTON achieves much faster training speed with the

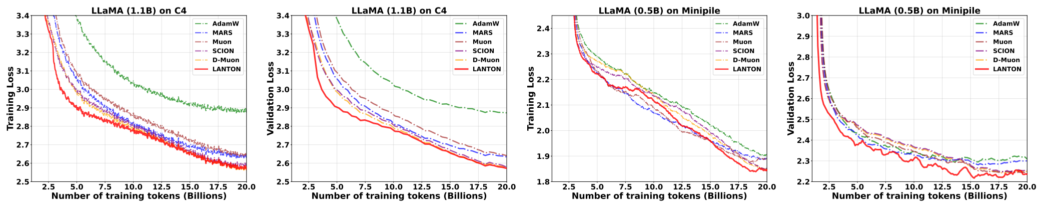

Figure 3: Training/validation loss on C4 and Minipile datasets.

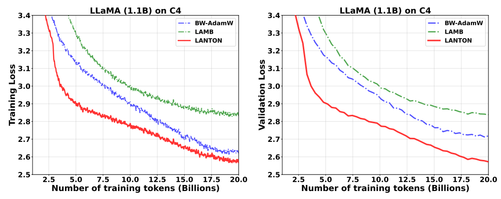

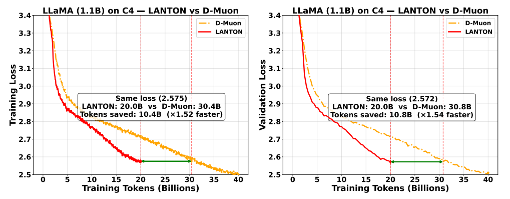

(a) Comparison with layer-/block-wise methods. (b) Comparison of sample efficiency.

Figure 4: Training/validation loss on C4 datasets. (a) Comparison with algorithms using layer-wise/block-wise learning rates. (b) LANTON shows higher sample efficiency than D-Muon.

same budget of training tokens, and exhibits 0.1 lower validation loss than BW-AdamW. LANTON adapts the noise-adaptive layer-wise learning rate on the fly by monitoring gradient noise, whereas BW-AdamW uses fixed step sizes per parameter group. Moreover, neither baseline explicitly considers the parameter geometry properties.

6.4 Sample Efficiency with Fixed Token Budget

To study the sample efficiency of our algorithm under various token budgets, we double the budget of tokens for D-Muon (i.e., 40B tokens) as that in LANTON (i.e., 20B tokens), and keep other experimental settings the same as that in Section 6.2.3, including the base learning rate, scale hyperparameters and batch size. Both algorithms use cosine learning rate decay, but the difference is that D-Muon has $2\times$ total training steps since it has $2\times$ more training tokens. Figure 4(b) shows that D-Muon and LANTON reach comparable training/validation losses when D-Muon uses about $1.5\times$ more tokens than LANTON (i.e., 30B tokens for D-Muon and 20B tokens for LANTON for reaching ~ 2.57 loss), demonstrating that the noise-adaptive learning rates can improve sample efficiency.

6.5 Robustness to Base Learning Rate Choice

To evaluate sensitivity to the base learning rate, we keep the model (LLaMA-1.1B), dataset (C4), batch size (1024), optimizer settings, and cosine schedule fixed, then train LANTON with various base learning rates $\eta_{\max} \in \{0.001, 0.003, 0.005\}$. We compare against the best tuned D-MUON under the same setup. As shown in Figure 7 in Appendix I, we find that for all learning rates except for $\eta_{\max} = 0.001$, LANTON consistently achieves equal or lower loss with fewer training tokens, i.e., converges faster. With $\eta_{\max} = 0.001$, LANTON's loss still decreases faster for most (70%) of the training trajectory, with the two methods becoming close only toward the end. Overall, LANTON demonstrates robust performance across base learning rates and superior convergence speed in most hyperparameter settings.

7 Conclusion

We propose LANTON, a geometry-aware optimizer that incorporates noise-adaptive layer-wise learning-rate scaling on the top of LMO-based updates. By estimating gradient variance in the dual norm space and rescaling learning rate across layers, LANTON accelerates the transformer training hindered by heterogeneous and evolving noise. Theoretically, we obtain a sharp convergence rate of $\tilde{O}(1/\sqrt{T} + \sqrt{\sum_\ell \bar{\sigma}_\ell}/T^{1/4})$ with improved noise dependence across layers. Empirically, LANTON accelerates pretraining and improves validation metrics on GPT2 and LLaMA under a fixed token budget. One limitation of our work is that the theoretical results may depend on the parameter dimension. Another limitation is that our experiments are conducted on moderately sized models; extending and validating the approach at larger scales is an important direction for future work.

Reproducibility Statement

We state the formal assumptions and results in the main text (Assumptions 5.1 and 5.2 and Theorem 5.3) and provide complete proofs of Theorem 5.3 in Appendices B and C. An anonymized code with training/evaluation scripts, configurations, seeds, and environment files is included in the supplementary materials. All base models are publicly available: LLaMA and GPT2-small/medium (used under their official research/community license; license text cited in Appendix N). Datasets C4, MiniPile, and OpenWebText are accessible on HuggingFace under the licenses stated on their corresponding Hugging Face dataset cards. We include download scripts, preprocessing/splits, and references to their dataset cards and licences (cited in Appendix N). These materials sufficiently support the reproduction of our results.

References

Josh Achiam, Steven Adler, Sandhini Agarwal, Lama Ahmad, Ilge Akkaya, Florencia Leoni Aleman, Diogo Almeida, Janko Altenschmidt, Sam Altman, Shyamal Anadkat, et al. Gpt-4 technical report. *arXiv preprint arXiv:2303.08774*, 2023.

Kwangjun Ahn, Byron Xu, Natalie Abreu, and John Langford. Dion: Distributed orthonormalized updates. *arXiv preprint arXiv:2504.05295*, 2025.

Rohan Anil, Vineet Gupta, Tomer Koren, Kevin Regan, and Yoram Singer. Scalable second order optimization for deep learning. *arXiv preprint arXiv:2002.09018*, 2020.

Jeremy Bernstein and Laker Newhouse. Modular duality in deep learning. *arXiv preprint arXiv:2410.21265*, 2024a.

Jeremy Bernstein and Laker Newhouse. Old optimizer, new norm: An anthology. *arXiv preprint arXiv:2409.20325*, 2024b.

Xiangning Chen, Chen Liang, Da Huang, Esteban Real, Kaiyuan Wang, Hieu Pham, Xuanyi Dong, Thang Luong, Cho-Jui Hsieh, Yifeng Lu, et al. Symbolic discovery of optimization algorithms. *Advances in neural information processing systems*, 36:49205–49233, 2023.

Ashok Cutkosky and Harsh Mehta. Momentum improves normalized sgd. In *International Conference on Machine Learning*, pp. 2260–2268. PMLR, 2020.

Ashok Cutkosky and Harsh Mehta. High-probability bounds for non-convex stochastic optimization with heavy tails. *Advances in Neural Information Processing Systems*, 34:4883–4895, 2021.

Aaron Defazio, Xingyu Yang, Ahmed Khaled, Konstantin Mishchenko, Harsh Mehta, and Ashok Cutkosky. The road less scheduled. *Advances in Neural Information Processing Systems*, 37: 9974–10007, 2024.

Jesse Dodge, Maarten Sap, Ana Marasović, William Agnew, Gabriel Ilharco, Dirk Groeneveld, Margaret Mitchell, and Matt Gardner. Documenting large webtext corpora: A case study on the colossal clean crawled corpus. *arXiv preprint arXiv:2104.08758*, 2021.

John Duchi, Elad Hazan, and Yoram Singer. Adaptive subgradient methods for online learning and stochastic optimization. *Journal of Machine Learning Research*, 12(Jul):2121–2159, 2011.

Marguerite Frank, Philip Wolfe, et al. An algorithm for quadratic programming. *Naval research logistics quarterly*, 3(1-2):95–110, 1956.

Leo Gao, Stella Biderman, Sid Black, Laurence Golding, Travis Hoppe, Charles Foster, Jason Phang, Horace He, Anish Thite, Noa Nabeshima, et al. The pile: An 800gb dataset of diverse text for language modeling. *arXiv preprint arXiv:2101.00027*, 2020.

Aaron Gokaslan, Vanya Cohen, Ellie Pavlick, and Stefanie Tellex. Openwebtext corpus. `http://Skylion007.github.io/OpenWebTextCorpus`, 2019.

Xiaochuan Gong, Jie Hao, and Mingrui Liu. Adaptive algorithms with sharp convergence rates for stochastic hierarchical optimization. *arXiv preprint arXiv:2509.15399*, 2025.

Vineet Gupta, Tomer Koren, and Yoram Singer. Shampoo: Preconditioned stochastic tensor optimization. In *International Conference on Machine Learning*, pp. 1842–1850. PMLR, 2018.

Nathan Halko, Per-Gunnar Martinsson, and Joel A Tropp. Finding structure with randomness: Probabilistic algorithms for constructing approximate matrix decompositions. *SIAM review*, 53 (2):217–288, 2011.

Maor Ivgi, Oliver Hinder, and Yair Carmon. Dog is sgd's best friend: A parameter-free dynamic step size schedule. In *International Conference on Machine Learning*, pp. 14465–14499. PMLR, 2023.

Martin Jaggi. Revisiting frank-wolfe: Projection-free sparse convex optimization. In *International conference on machine learning*, pp. 427–435. PMLR, 2013.

Keller Jordan, Yuchen Jin, Vlado Boza, You Jiacheng, Franz Cesista, Laker Newhouse, and Jeremy Bernstein. Muon: An optimizer for hidden layers in neural networks, 2024. URL `https://kellerjordan.github.io/posts/muon/`.

Jean Kaddour. The minipile challenge for data-efficient language models. *arXiv preprint arXiv:2304.08442*, 2023.

Diederik P Kingma and Jimmy Ba. Adam: A method for stochastic optimization. *International Conference on Learning Representations (ICLR)*, 2014.

Tim Large, Yang Liu, Minyoung Huh, Hyojin Bahng, Phillip Isola, and Jeremy Bernstein. Scalable optimization in the modular norm. *Advances in Neural Information Processing Systems*, 37: 73501–73548, 2024.

Jiaxiang Li and Mingyi Hong. A note on the convergence of muon. *arXiv preprint arXiv:2502.02900*, 2025.

Hong Liu, Zhiyuan Li, David Hall, Percy Liang, and Tengyu Ma. Sophia: A scalable stochastic second-order optimizer for language model pre-training. *arXiv preprint arXiv:2305.14342*, 2023a.

Jingyuan Liu, Jianlin Su, Xingcheng Yao, Zhejun Jiang, Guokun Lai, Yulun Du, Yidao Qin, Weixin Xu, Enzhe Lu, Junjie Yan, et al. Muon is scalable for llm training. *arXiv preprint arXiv:2502.16982*, 2025.

Zijian Liu, Srikanth Jagabathula, and Zhengyuan Zhou. Near-optimal non-convex stochastic optimization under generalized smoothness. *arXiv preprint arXiv:2302.06032*, 2023b.

Zijian Liu, Srikanth Jagabathula, and Zhengyuan Zhou. Near-optimal non-convex stochastic optimization under generalized smoothness. *arXiv preprint arXiv:2302.0603*, 2023c.

Ilya Loshchilov and Frank Hutter. Decoupled weight decay regularization. *arXiv preprint arXiv:1711.05101*, 2017.

Sadhika Malladi, Tianyu Gao, Eshaan Nichani, Alex Damian, Jason D Lee, Danqi Chen, and Sanjeev Arora. Fine-tuning language models with just forward passes. *Advances in Neural Information Processing Systems*, 36:53038–53075, 2023.

James Martens and Roger Grosse. Optimizing neural networks with kronecker-factored approximate curvature. In *International conference on machine learning*, pp. 2408–2417. PMLR, 2015.

Konstantin Mishchenko and Aaron Defazio. Prodigy: An expeditiously adaptive parameter-free learner. *arXiv preprint arXiv:2306.06101*, 2023.

Tae-Hyun Oh, Yasuyuki Matsushita, Yu-Wing Tai, and In So Kweon. Fast randomized singular value thresholding for nuclear norm minimization. In *Proceedings of the IEEE Conference on Computer Vision and Pattern Recognition*, pp. 4484–4493, 2015.

Matteo Pagliardini, Pierre Ablin, and David Grangier. The ademamix optimizer: Better, faster, older. *arXiv preprint arXiv:2409.03137*, 2024.

Thomas Pethick, Wanyun Xie, Kimon Antonakopoulos, Zhenyu Zhu, Antonio Silveti-Falls, and Volkan Cevher. Training deep learning models with norm-constrained lmos. *arXiv preprint arXiv:2502.07529*, 2025.

Alec Radford, Jeffrey Wu, Rewon Child, David Luan, Dario Amodei, Ilya Sutskever, et al. Language models are unsupervised multitask learners. *OpenAI blog*, 1(8):9, 2019.

Artem Riabinin, Egor Shulgin, Kaja Gruntkowska, and Peter Richtárik. Gluon: Making muon & scion great again!(bridging theory and practice of lmo-based optimizers for llms). *arXiv preprint arXiv:2505.13416*, 2025.

Herbert Robbins and Sutton Monro. A stochastic approximation method. *The annals of mathematical statistics*, pp. 400–407, 1951.

Noam Shazeer and Mitchell Stern. Adafactor: Adaptive learning rates with sublinear memory cost. In *International Conference on Machine Learning*, pp. 4596–4604. PMLR, 2018.

Wei Shen, Ruichuan Huang, Minhui Huang, Cong Shen, and Jiawei Zhang. On the convergence analysis of muon. *arXiv preprint arXiv:2505.23737*, 2025.

Hao-Jun Michael Shi, Tsung-Hsien Lee, Shintaro Iwasaki, Jose Gallego-Posada, Zhijing Li, Kaushik Rangadurai, Dheevatsa Mudigere, and Michael Rabbat. A distributed data-parallel pytorch implementation of the distributed shampoo optimizer for training neural networks at-scale. *arXiv preprint arXiv:2309.06497*, 2023.

Chongjie Si, Debing Zhang, and Wei Shen. Adamuon: Adaptive muon optimizer. *arXiv e-prints*, pp. arXiv–2507, 2025.

Tijmen Tieleman and Geoffrey Hinton. Lecture 6.5-rmsprop, coursera: Neural networks for machine learning. *University of Toronto, Technical Report*, 6, 2012.

Hugo Touvron, Thibaut Lavril, Gautier Izacard, Xavier Martinet, Marie-Anne Lachaux, Timothée Lacroix, Baptiste Rozière, Naman Goyal, Eric Hambro, Faisal Azhar, et al. Llama: Open and efficient foundation language models. *arXiv preprint arXiv:2302.13971*, 2023.

Nikhil Vyas, Depen Morwani, Rosie Zhao, Mujin Kwun, Itai Shapira, David Brandfonbrener, Lucas Janson, and Sham Kakade. Soap: Improving and stabilizing shampoo using adam. *arXiv preprint arXiv:2409.11321*, 2024.

Jinbo Wang, Mingze Wang, Zhanpeng Zhou, Junchi Yan, Lei Wu, et al. The sharpness disparity principle in transformers for accelerating language model pre-training. *arXiv preprint arXiv:2502.19002*, 2025.

Yang You, Igor Gitman, and Boris Ginsburg. Scaling sgd batch size to 32k for imagenet training. *arXiv preprint arXiv:1708.03888*, 6:12, 2017.

Yang You, Jing Li, Sashank Reddi, Jonathan Hseu, Sanjiv Kumar, Srinadh Bhojanapalli, Xiaodan Song, James Demmel, Kurt Keutzer, and Cho-Jui Hsieh. Large batch optimization for deep learning: Training bert in 76 minutes. *arXiv preprint arXiv:1904.00962*, 2019.

Huizhuo Yuan, Yifeng Liu, Shuang Wu, Xun Zhou, and Quanquan Gu. Mars: Unleashing the power of variance reduction for training large models. *arXiv preprint arXiv:2411.10438*, 2024.

Matthew D Zeiler. Adadelta: an adaptive learning rate method. *arXiv preprint arXiv:1212.5701*, 2012.

Yushun Zhang, Congliang Chen, Ziniu Li, Tian Ding, Chenwei Wu, Diederik P Kingma, Yinyu Ye, Zhi-Quan Luo, and Ruoyu Sun. Adam-mini: Use fewer learning rates to gain more. *arXiv preprint arXiv:2406.16793*, 2024.

Jiawei Zhao, Zhenyu Zhang, Beidi Chen, Zhangyang Wang, Anima Anandkumar, and Yuandong Tian. Galore: Memory-efficient llm training by gradient low-rank projection. In *International Conference on Machine Learning*, pp. 61121–61143. PMLR, 2024a.

Rosie Zhao, Depen Morwani, David Brandfonbrener, Nikhil Vyas, and Sham Kakade. Deconstructing what makes a good optimizer for language models. *arXiv preprint arXiv:2407.07972*, 2024b.

A Technical Lemmas

In this section, we state several standard probabilistic and norm-equivalence lemmas without proof.

Lemma A.1 (Azuma-Hoeffding inequality). *Let $\{Z_t\}_{t\ge 0}$ be a martingale with respect to filtration $\{\mathcal{F}_t\}_{t\ge 0}$. Assume that $|Z_t - Z_{t-1}| \le c_t$ almost surely for all $t \ge 0$. Then for any fixed T, with probability at least $1-\delta$,*

$$|Z_T - Z_0| \le \sqrt{2\sum_{t=1}^{T} c_t^2 \log(2/\delta)}.$$

Lemma A.2 ((Liu et al., 2023c, Lemma 2.4)). *Suppose $X_1, \dots, X_T$ is a martingale difference sequence adapted to a filtration $\mathcal{F}_1, \dots, \mathcal{F}_T$ in a Hilbert space such that $\|X_t\|_F \le R_t$ almost surely for some $R_t \ge 0$. Then for any $\delta \in (0,1)$, with probability at least $1-\delta$, for any fixed t we have*

$$\left\|\sum_{s=1}^{t} X_s\right\|_F \le 4\sqrt{\log\frac{2}{\delta}\sum_{s=1}^{T} R_s^2}.$$

Proof of Lemma A.2. Since $\|\cdot\|_F$ satisfies $\|X+Y\|_F^2 \le \|X\|_F^2 + \langle \nabla\|X\|_F^2, Y\rangle + \|Y\|_F^2$ for all X, Y, the condition for applying (Cutkosky & Mehta, 2021, Lemma 10) is satisfied, and therefore (Liu et al., 2023c, Lemma 2.4) holds. □

Lemma A.3 (Equivalence of norms). *For any two matrix norms $\|\cdot\|_a$ and $\|\cdot\|_b$, there exists $0 < C_1 \le C_2$ (with $C_2 \ge 1$) such that $C_1\|A\|_a \le \|A\|_b \le C_2\|A\|_a$ for all matrices $A \in \mathbb{R}^{m\times n}$.*

Remark A.4. In the subsequent analysis, we will use the relationship among Frobenius norm $\|\cdot\|_F$, spectral norm $\|\cdot\|_2$, and nuclear norm $\|\cdot\|_{\text{nuc}}$. Specifically, for $A \in \mathbb{R}^{m\times n}$ we have

- $\|A\|_2 \le \|A\|_F \le \sqrt{\text{rank}(A)}\|A\|_2 \implies C_1 \le 1, C_2 \ge \sqrt{\max\{m,n\}}$.
- $\|A\|_{\text{nuc}}/\sqrt{\text{rank}(A)} \le \|A\|_F \le \|A\|_{\text{nuc}} \implies C_1 \le 1/\sqrt{\max\{m,n\}}, C_2 \ge 1$.

B Proofs of Section 5.1

We first recall a few key definitions from Equation (1) (with the convention $0/0 := 1$):

$$\kappa_\sigma^\ell = \begin{cases} \bar\sigma_\ell/\underline{\sigma}_\ell & \underline{\sigma}_\ell > 0 \\ 1 & \bar\sigma_\ell = 0 \end{cases}, \quad \kappa_\sigma = \max_\ell \kappa_\sigma^\ell, \quad \bar\sigma_{\max} = \max_\ell \bar\sigma_\ell, \quad \text{and} \quad t_0 = \frac{\log 2}{\log(1/\beta_2)}. \tag{5}$$

The following proofs are based on Assumptions 5.1 and 5.2 and the setting of Theorem 5.3. For simplicity, we omit the ℓ superscript/subscript whenever the context is clear.

Lemma 5.4. *With probability at least $1-\delta$, for all ℓ and $t_0 \le t \le T$, $\frac{\underline{\sigma}_\ell^2(1-\beta_2^t)}{C_2} \le H_t^\ell \le 4\bar\sigma_\ell^2(1-\beta_2^t)$.*

Proof of Lemma 5.4. Consider the case where $0 < \underline{\sigma} \le \bar\sigma$. Denote $c_{t,k} = \beta_2^{t-k}(1-\beta_2)$. By Assumption 5.2 and Young's inequality,

$$H_t = \sum_{k=1}^{t} c_{t,k}\|G_k - \tilde G_k\|_*^2 \le 2\sum_{k=1}^{t} c_{t,k}\left(\|G_k - \nabla f(X_t)\|_*^2 + \|\tilde G_t - \nabla f(X_t)\|_*^2\right)$$

$$\le 4\bar\sigma^2 \sum_{k=1}^{t} c_{t,k} = 4\bar\sigma^2 \sum_{k=1}^{t} \beta_2^{t-k}(1-\beta_2) = 4\bar\sigma^2(1-\beta_2^t). \tag{6}$$

We proceed to derive high probability lower bound for $\sum_{k=1}^{t} c_{t,k}\|G_k - \tilde G_k\|_F^2$. Denote $\sigma_k^2 = \mathbb{E}_{k-1}[\|G_k - \nabla f(X_k)\|_F^2]$. Let $Z_k = c_{t,k}(\|G_k - \tilde G_k\|_F^2 - 2\sigma_k^2)$, then $\{Z_k\}_{k\ge 1}$ is a martingale difference sequence since

$$\mathbb{E}_{k-1}[Z_k] = \mathbb{E}_{t-1}[\|G_k - \tilde G_k\|_F^2 - 2\sigma_k^2]$$

$$
\begin{aligned}
&= \mathbb{E}_{t-1}[\|G_k - \nabla f(X_k)\|_F^2 + \|\tilde{G}_k - \nabla f(X_k)\|_F^2 - 2\langle G_k - \nabla f(X_k), \tilde{G}_k - \nabla f(X_k)\rangle] - 2\sigma_k^2 \\
&= 0.
\end{aligned}
$$

Using Assumption 5.2 and Lemma A.3 and Young's inequality, we have $Z_k \geq -2c_{t,k}\sigma_k^2$ and

$$
Z_k \leq c_{t,k}\left(2C_2\left(\|G_k - \nabla f(X_k)\|_*^2 + \|\tilde{G}_k - \nabla f(X_k)\|_*^2\right) - 2\sigma_k^2\right) \leq c_{t,k}(4C_2\bar{\sigma}^2 - 2\sigma_k^2).
$$

This implies that

$$
|Z_k| \leq c_{t,k} \cdot \max\left\{2\sigma_k^2, 4C_2\bar{\sigma}^2 - 2\sigma_k^2\right\} = c_{t,k}(4C_2\bar{\sigma}^2 - 2\sigma_k^2),
$$

where the last equality is due to $C_2 \geq 1$ and $\sigma_k \leq \bar{\sigma}$ almost surely. Then by the Azuma-Hoeffding inequality (Lemma A.1) and a union bound over t, for any $\delta \in (0,1)$, with probability at least $1-\delta$, for all $t \leq T$,

$$
\left|\sum_{k=1}^{t} Z_k\right| \leq \sqrt{2\sum_{k=1}^{t}(c_{t,k}(4C_2\bar{\sigma}^2 - 2\sigma_k^2))^2 \log\frac{2T}{\delta}} \leq (4C_2\bar{\sigma}^2 - 2\underline{\sigma}^2)\sqrt{\frac{2(1-\beta_2)}{1+\beta_2}\log\frac{2T}{\delta}}. \quad (7)
$$

Rearranging Equation (7) yields that, with probability at least $1-\delta$, for all $t \leq T$,

$$
\begin{aligned}
\sum_{k=1}^{t} c_{t,k}\|G_k - \tilde{G}_k\|_F^2 &\geq 2\sum_{k=1}^{t} c_{t,k}\sigma_k^2 - (4C_2\bar{\sigma}^2 - 2\underline{\sigma}^2)\sqrt{\frac{2(1-\beta_2)}{1+\beta_2}\log\frac{2T}{\delta}} \\
&\geq 2\underline{\sigma}^2(1-\beta_2^t) - (4C_2\bar{\sigma}^2 - 2\underline{\sigma}^2)\sqrt{\frac{2(1-\beta_2)}{1+\beta_2}\log\frac{2T}{\delta}}.
\end{aligned}
$$

By the choice of β_2 in Theorem 5.3 and the definition of t_0, for all $t \geq t_0$ we have

$$
\frac{4C_2\bar{\sigma}^2 - 2\underline{\sigma}^2}{\underline{\sigma}^2}\sqrt{\frac{2(1-\beta_2)}{1+\beta_2}\log\frac{2T}{\delta}} \leq \frac{1}{2} \quad \text{and} \quad (4C_2\bar{\sigma}^2 - 2\underline{\sigma}^2)\sqrt{\frac{2(1-\beta_2)}{1+\beta_2}\log\frac{2T}{\delta}} \leq \underline{\sigma}^2(1-\beta_2^t).
$$

Therefore, by Lemma A.3, with probability at least $1-\delta$, for all $t_0 \leq t \leq T$,

$$
\sum_{k=1}^{t} c_{t,k}\|G_k - \tilde{G}_k\|_F^2 \geq \underline{\sigma}^2(1-\beta_2^t) \implies \sum_{k=1}^{t} c_{t,k}\|G_k - \tilde{G}_k\|_*^2 \geq \frac{\underline{\sigma}^2(1-\beta_2^t)}{C_2}. \quad (8)
$$

We conclude the proof by combining Equations (6) and (8) and noting that the results also hold for the case $\underline{\sigma} = \bar{\sigma} = 0$. □

Lemma 5.5. *With probability at least $1-\delta$, for all ℓ and $t \leq T$,*

$$
\min\left\{\frac{\alpha}{\sqrt{\alpha^2 + 4\bar{\sigma}_{\max}^2}}, \frac{1}{2\sqrt{C_2}\kappa_\sigma}\right\} =: \alpha_r \leq \frac{\alpha_t^\ell}{\alpha_t^m} \leq 1, \quad (2)
$$

and therefore, with probability at least $1-\delta$, we have $\alpha_r\eta_{\min} \leq \eta_t^\ell \leq \eta_{\max}$ for all ℓ and $t \leq T$.

Proof of Lemma 5.5. By Lemma 5.4, for all $t_0 \leq t \leq T$, it holds with probability at least $1-\delta$ that

$$
\frac{\underline{\sigma}^2(1-\beta_2^t)}{C_2} \leq \sum_{k=1}^{t}\beta_2^{t-k}(1-\beta_2)\|G_k - \tilde{G}_k\|_*^2 \leq 4\bar{\sigma}^2(1-\beta_2^t).
$$

Therefore, with probability at least $1-\delta$, for all ℓ and $t \leq T$,

$$
\frac{\alpha}{\sqrt{\alpha^2 + 4\bar{\sigma}^2(1-\beta_2^t)}} \leq \alpha_t^\ell \leq \mathbb{I}(t < t_0) + \frac{\alpha}{\sqrt{\alpha^2 + \underline{\sigma}^2(1-\beta_2^t)/C_2}}\mathbb{I}(t \geq t_0). \quad (9)
$$

Using Equation (9), we have

$$
\frac{\alpha_t^\ell}{\alpha_t^m} \geq \frac{\alpha}{\sqrt{\alpha^2 + 4\bar{\sigma}^2(1-\beta_2^t)}}\left(\mathbb{I}(t < t_0) + \frac{\alpha}{\sqrt{\alpha^2 + \underline{\sigma}^2(1-\beta_2^t)/C_2}}\mathbb{I}(t \geq t_0)\right)^{-1}
$$

$$= \frac{\alpha}{\sqrt{\alpha^2 + 4\bar{\sigma}^2(1-\beta_2^t)}}\mathbb{I}(t < t_0) + \frac{\sqrt{\alpha^2 + \underline{\sigma}^2(1-\beta_2^t)/C_2}}{\sqrt{\alpha^2 + 4\bar{\sigma}^2(1-\beta_2^t)}}\mathbb{I}(t \geq t_0)$$
$$\geq \frac{\alpha}{\sqrt{\alpha^2 + 4\bar{\sigma}^2(1-\beta_2^t)}}\mathbb{I}(t < t_0) + \frac{\underline{\sigma}}{2\sqrt{C_2}\bar{\sigma}}\mathbb{I}(t \geq t_0) \geq \min\left\{\frac{\alpha}{\sqrt{\alpha^2+4\bar{\sigma}^2}}, \frac{\underline{\sigma}}{2\sqrt{C_2}\bar{\sigma}}\right\},$$

that is (we add back the subscript ℓ here),

$$\min\left\{\frac{\alpha}{\sqrt{\alpha^2+4\bar{\sigma}_\ell^2}}, \frac{\underline{\sigma}_\ell}{2\sqrt{C_2}\bar{\sigma}_\ell}\right\} =: \alpha_r^\ell \leq \frac{\alpha_t^\ell}{\alpha_t^m} \leq 1.$$

Let $\alpha_r = \min_\ell \alpha_r^\ell$, and recall the definitions of $\bar{\sigma}_{\max}$ and κ_σ in Equation (5), then for all ℓ,

$$\min\left\{\frac{\alpha}{\sqrt{\alpha^2+4\bar{\sigma}_{\max}^2}}, \frac{1}{2\sqrt{C_2}\kappa_\sigma}\right\} =: \alpha_r \leq \frac{\alpha_t^\ell}{\alpha_t^m} \leq 1,$$

which gives Equation (2). The proof is completed. □

C Proof of Theorem 5.3

Before proving Theorem 5.3, we first provide a descent lemma for Algorithm 1.

Lemma C.1. *For the update in Algorithm 1, we have*

$$f(X_{t+1}) \leq f(X_t) + \sum_{\ell=1}^p \left(-\eta_t^\ell \|\nabla_\ell f(X_t)\|_{(\ell)*} + 2\eta_t^\ell \|B_t^\ell - \nabla_\ell f(X_t)\|_{(\ell)*} + \frac{L_\ell}{2}(\eta_t^\ell)^2\right).$$

Moreover, we have

$$\sum_{t=1}^T \sum_{\ell=1}^p \eta_t^\ell \|\nabla_\ell f(X_t)\|_{(\ell)*} \leq f(X_1) - f^* + \sum_{t=1}^T \sum_{\ell=1}^p \left(2\eta_t^\ell \|B_t^\ell - \nabla_\ell f(X_t)\|_{(\ell)*} + \frac{L_\ell}{2}(\eta_t^\ell)^2\right).$$

Proof of Lemma C.1. Applying (Riabinin et al., 2025, Lemma 1) with $X = X_t$ and $Y = X_{t+1}$,

$$f(X_{t+1}) \leq f(X_t) + \langle \nabla f(X_t), X_{t+1} - X_t\rangle + \sum_{\ell=1}^p \frac{L_\ell}{2}\|X_{t+1}^\ell - X_t^\ell\|_{(\ell)}^2$$
$$= f(X_t) + \sum_{\ell=1}^p \left(\langle \nabla_\ell f(X_t), X_{t+1}^\ell - X_t^\ell\rangle + \frac{L_\ell}{2}(\eta_t^\ell)^2\right).$$

For the second term, using the update of X_{t+1}^ℓ and the Cauchy-Schwarz inequality we have

$$\begin{aligned}\langle \nabla_\ell f(X_t), X_{t+1}^\ell - X_t^\ell\rangle &= \langle B_t^\ell, X_{t+1}^\ell - X_t^\ell\rangle + \langle \nabla_\ell f(X_t) - B_t^\ell, X_{t+1}^\ell - X_t^\ell\rangle \\ &\leq -\eta_t^\ell \|B_t^\ell\|_{(\ell)*} + \eta_t^\ell \|\nabla_\ell f(X_t) - B_t^\ell\|_{(\ell)*} \\ &\leq -\eta_t^\ell \|\nabla_\ell f(X_t)\|_{(\ell)*} + 2\eta_t^\ell \|B_t^\ell - \nabla_\ell f(X_t)\|_{(\ell)*}.\end{aligned}$$

Therefore, we obtain

$$f(X_{t+1}) \leq f(X_t) + \sum_{\ell=1}^p \left(-\eta_t^\ell \|\nabla_\ell f(X_t)\|_{(\ell)*} + 2\eta_t^\ell \|B_t^\ell - \nabla_\ell f(X_t)\|_{(\ell)*} + \frac{L_\ell}{2}(\eta_t^\ell)^2\right).$$

Rearranging the terms and taking summation over t gives the result. □

Theorem 5.3. *Suppose Assumptions 5.1 and 5.2 hold. Let $\Delta_1 = f(X_1) - f^*$. Set $\beta_1 = 1-\alpha$ with $\alpha = \min\left(\frac{\sqrt{\Delta_1 \sum_\ell L_\ell}}{\sum_\ell \bar{\sigma}_\ell \sqrt{T}}, 1\right)$, $1 - \min_\ell \frac{\underline{\sigma}_\ell^4}{32(2C_2\bar{\sigma}_\ell^2 - \underline{\sigma}_\ell^2)^2 \log(4T/\delta)} \leq \beta_2 < 1$, $\eta_{\max} = \sqrt{\frac{\Delta_1 \alpha}{\sum_\ell L_\ell T}}$, and $\eta_{\min} = \eta_{\max}/\kappa_\eta$ with $1 \leq \kappa_\eta \leq O(1)$. With probability at least $1-\delta$, we have*

$$\frac{1}{T}\sum_{t=1}^T \sum_{\ell=1}^p \|\nabla_\ell f(X_t)\|_{(\ell)*} \lesssim \frac{\sqrt{C_2}(\sum_\ell \bar{\sigma}_\ell)^2}{\sqrt{\Delta_1 \sum_\ell L_\ell T}} + \frac{C_2^{3/2}}{C_1}\sqrt{\log\frac{T}{\delta}}\left(\frac{\sqrt{\Delta_1 \sum_\ell L_\ell}}{\sqrt{T}} + \frac{\sqrt{\sum_\ell \bar{\sigma}_\ell}(\Delta_1 \sum_\ell L_\ell)^{1/4}}{T^{1/4}}\right).$$

Proof of Theorem 5.3. Define $\hat{\epsilon}_t^\ell = B_t^\ell - \nabla_\ell f(X_t)$, $\epsilon_t^\ell = G_t^\ell - \nabla_\ell f(X_t)$, and $S(X,Y) = \nabla f(X) - \nabla f(Y)$. Check that

$$\begin{aligned}\hat{\epsilon}_{t+1}^\ell &= \beta_1 \hat{\epsilon}_t^\ell + (1-\beta_1)\epsilon_t^\ell + S(X_t^\ell, X_{t+1}^\ell)\\ &= \beta_1^t \hat{\epsilon}_1^\ell + (1-\beta_1)\sum_{\tau=0}^{t-1}\beta_1^\tau \epsilon_{t-\tau}^\ell + \sum_{\tau=0}^{t-1}\beta_1^\tau S(X_{t-\tau}^\ell, X_{t+1-\tau}^\ell).\end{aligned}$$

Using L-smoothness, $\|S(X_t^\ell) - S(X_{t+1}^\ell)\|_{(\ell)*} \le L_\ell \|X_{t+1}^\ell - X_t^\ell\|_{(\ell)} = L_\ell \eta_t^\ell \|O_t^\ell\|_{(\ell)} = L_\ell \eta_t^\ell$, and $\eta_t^\ell \le \eta_{\max}$ by Lemma 5.5,

$$\|\hat{\epsilon}_{t+1}^\ell\|_{(\ell)*} \le \beta_1^t \|\hat{\epsilon}_1^\ell\|_{(\ell)*} + (1-\beta_1)\left\|\sum_{\tau=0}^{t-1}\beta_1^\tau \epsilon_{t-\tau}^\ell\right\|_{(\ell)*} + \eta_{\max} L_\ell \sum_{\tau=0}^{t-1}\beta_1^\tau.$$

Applying Lemma A.2 with $R_\tau = C_2 \beta_1^\tau \bar{\sigma}_\ell$ since $\|\beta_1^\tau \epsilon_{t-\tau}^\ell\|_F \le C_2 \|\beta_1^\tau \epsilon_{t-\tau}^\ell\|_{(\ell)*} \le C_2 \beta_1^\tau \bar{\sigma}_\ell$, a union bound over t, and Lemma A.3, with probability at least $1-\delta$, for all $t \le T$,

$$\left\|\sum_{\tau=0}^{t-1}\beta_1^\tau \epsilon_{t-\tau}^\ell\right\|_{(\ell)*} \le \frac{1}{C_1}\left\|\sum_{\tau=0}^{t-1}\beta_1^\tau \epsilon_{t-\tau}^\ell\right\|_F \le \frac{4}{C_1}\sqrt{\log\frac{2T}{\delta}\sum_{\tau=0}^{t-1}(C_2\beta_1^\tau \bar{\sigma}_\ell)^2} \le \frac{4C_2\bar{\sigma}_\ell}{C_1}\sqrt{\frac{\log(2T/\delta)}{1-\beta_1}}.$$

Therefore, observing that $\hat{\epsilon}_1^\ell = \epsilon_1^\ell$ and plugging in the concentration bound yields

$$\|\hat{\epsilon}_{t+1}^\ell\|_{(\ell)*} \le \beta_1^t \bar{\sigma}_\ell + \frac{4C_2}{C_1}(1-\beta_1)\bar{\sigma}_\ell\sqrt{\frac{\log(2T/\delta)}{1-\beta_1}} + \frac{\eta_{\max}L_\ell}{1-\beta_1}.$$

Taking summation, with probability at least $1-\delta$ we have

$$\sum_{t=1}^T \|\hat{\epsilon}_t^\ell\|_{(\ell)*} \le \frac{\bar{\sigma}_\ell}{1-\beta_1} + \frac{4C_2}{C_1}T\sqrt{1-\beta_1}\,\bar{\sigma}_\ell\sqrt{\log\frac{2T}{\delta}} + \frac{T\eta_{\max}L_\ell}{1-\beta_1}. \tag{10}$$

Recall Lemma C.1 and the definitions of Δ_1 and $\hat{\epsilon}_t^\ell$,

$$\sum_{t=1}^T\sum_{\ell=1}^p \eta_t^\ell \|\nabla_\ell f(X_t)\|_{(\ell)*} \le \Delta_1 + \sum_{t=1}^T\sum_{\ell=1}^p\left(2\eta_t^\ell \|\hat{\epsilon}_t^\ell\|_{(\ell)*} + \frac{L_\ell}{2}(\eta_t^\ell)^2\right).$$

By Lemma 5.5 and a union bound (with Equation (10)), with probability at least $1-2\delta$,

$$\begin{aligned}\sum_{t=1}^T\sum_{\ell=1}^p \|\nabla_\ell f(X_t)\|_{(\ell)*} &\le \frac{\Delta_1}{\alpha_r\eta_{\min}} + \sum_{\ell=1}^p\left(\frac{2\eta_{\max}}{\alpha_r\eta_{\min}}\sum_{t=1}^T\|\nabla_\ell f(X_t) - B_t^\ell\| + \frac{\eta_{\max}^2}{2\alpha_r\eta_{\min}}L_\ell T\right)\\ &\le \frac{\kappa_\eta\Delta_1}{\alpha_r\eta_{\max}} + \sum_{\ell=1}^p\left(\frac{2\kappa_\eta}{\alpha_r}\left(\frac{\bar{\sigma}_\ell}{1-\beta_1} + \frac{4C_2}{C_1}T\sqrt{1-\beta_1}\,\bar{\sigma}_\ell\sqrt{\log\frac{2T}{\delta}}\right) + \frac{\kappa_\eta\eta_{\max}}{\alpha_r}\left(\frac{2TL_\ell}{1-\beta_1} + \frac{L_\ell T}{2}\right)\right)\\ &\le \frac{\kappa_\eta\Delta_1}{\alpha_r\eta_{\max}} + \frac{2\kappa_\eta}{\alpha_r}\left(\frac{\sum_\ell\bar{\sigma}_\ell}{1-\beta_1} + \frac{4C_2}{C_1}T\sqrt{1-\beta_1}\sum_\ell\bar{\sigma}_\ell\sqrt{\log\frac{2T}{\delta}}\right) + \frac{5\kappa_\eta\eta_{\max}T\sum_\ell L_\ell}{\alpha_r(1-\beta_1)}\\ &\le \frac{6\kappa_\eta}{\alpha_r}\sqrt{\frac{\Delta_1\sum_\ell L_\ell T}{1-\beta_1}} + \frac{2\kappa_\eta}{\alpha_r}\left(\frac{\sum_\ell\bar{\sigma}_\ell}{1-\beta_1} + \frac{4C_2}{C_1}T\sqrt{1-\beta_1}\sum_\ell\bar{\sigma}_\ell\sqrt{\log\frac{2T}{\delta}}\right)\\ &\le \left(\frac{6\kappa_\eta}{\alpha_r} + \frac{2\kappa_\eta}{\alpha_r}\left(1 + \frac{4C_2}{C_1}\sqrt{\log\frac{2T}{\delta}}\right)\right)\sqrt{\Delta_1\sum_\ell L_\ell T} + \frac{2\kappa_\eta(\sum_\ell\bar{\sigma}_\ell)^2\sqrt{T}}{\alpha_r\sqrt{\Delta_1\sum_\ell L_\ell}}\\ &\quad + \left(\frac{6\kappa_\eta}{\alpha_r} + \frac{8C_2\kappa_\eta}{C_1\alpha_r}\sqrt{\log\frac{2T}{\delta}}\right)\sqrt{\sum_\ell\bar{\sigma}_\ell}\left(\Delta_1\sum_\ell L_\ell\right)^{1/4}T^{3/4},\end{aligned}$$

where the last two inequalities use the choice of $\eta_{\max}$ and β_1 as stated in Theorem 5.3. Therefore, we obtain with probability at least $1-2\delta$ that

$$\frac{1}{T}\sum_{t=1}^T\sum_{\ell=1}^p \|\nabla_\ell f(X_t)\|_{(\ell)*} \le \left(\frac{6\kappa_\eta}{\alpha_r} + \frac{2\kappa_\eta}{\alpha_r}\left(1 + \frac{4C_2}{C_1}\sqrt{\log\frac{2T}{\delta}}\right)\right)\frac{\sqrt{\Delta_1\sum_\ell L_\ell}}{\sqrt{T}} + \frac{2\kappa_\eta(\sum_\ell\bar{\sigma}_\ell)^2}{\alpha_r\sqrt{\Delta_1\sum_\ell L_\ell T}}$$

$$+\left(\frac{6\kappa_\eta}{\alpha_r}+\frac{8C_2\kappa_\eta}{C_1\alpha_r}\sqrt{\log\frac{2T}{\delta}}\right)\frac{\sqrt{\sum_\ell \bar{\sigma}_\ell}(\Delta_1\sum_\ell L_\ell)^{1/4}}{T^{1/4}}.$$

Recall the definition of κ_σ and α_r in Equations (2) and (5), with probability at least $1-2\delta$,

$$\frac{1}{T}\sum_{t=1}^{T}\sum_{\ell=1}^{p}\|\nabla_\ell f(X_t)\|_{(\ell)*}\le \kappa_\eta \max\left\{\sqrt{1+\frac{4\bar{\sigma}_{\max}^2}{\alpha^2}},2\sqrt{C_2}\kappa_\sigma\right\}\left(\left(8+\frac{8C_2}{C_1}\sqrt{\log\frac{2T}{\delta}}\right)\frac{\sqrt{\Delta_1\sum_\ell L_\ell}}{\sqrt{T}}\right.$$
$$\left.+\frac{2(\sum_\ell\bar{\sigma}_\ell)^2}{\sqrt{\Delta_1\sum_\ell L_\ell T}}+\left(6+\frac{8C_2}{C_1}\sqrt{\log\frac{2T}{\delta}}\right)\frac{\sqrt{\sum_\ell\bar{\sigma}_\ell}(\Delta_1\sum_\ell L_\ell)^{1/4}}{T^{1/4}}\right).$$

Replacing δ with $\delta/2$ completes the proof. □

D Experiment of Image Classification

Following airbench setting in `https://github.com/KellerJordan/cifar10-airbench` and `https://github.com/LIONS-EPFL/scion/tree/main/examples/airbench`, we evaluate LANTON on CIFAR-100 image classification using an 8-layer convolutional neural network (CNN). Since stochastic gradient descent (SGD) generally outperforms AdamW on vision tasks, we follow the prior airbench setup and apply SGD to the norm and bias parameters for both Muon and D-Muon. LANTON partitions the parameters into two groups: (1) convolutional layers (matrix parameters), and (2) norm-layer and bias parameters. Newton–Schulz iterations are applied to the convolutional layers, while sign momentum is used for the norm and bias parameters. The full hyperparameter configuration is provided in Table XXX of the appendix.

As shown in Figure 5, all optimizers eventually reach nearly 100% training accuracy on airbench CIFAR-100. However, LANTON exhibits a significantly faster convergence rate than other baselines: it reaches almost maximal training accuracy by around 70 epochs. More importantly, LANTON consistently achieves the highest validation accuracy, demonstrating that LANTON not only accelerates optimization throughout the training process but also yields superior generalization performance compared to all baselines.

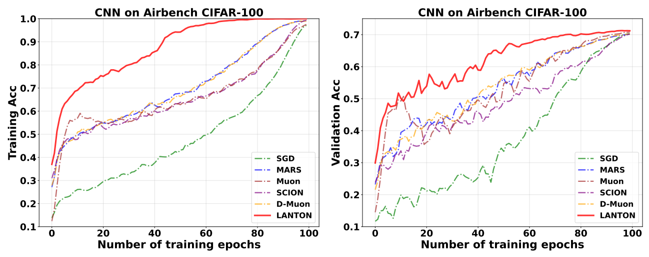

Figure 5: Training/validation accuracy on CIFAR-100.

Table 2: The hyperparameter settings in image classification.

Method	$\eta_{\max}$	Moment
SGD	0.1	$\beta=0.85$
Muon	0.24	$\beta_1=0.6,\beta_2=0.85,\beta_3=0.95$
MARS	0.1	$\beta_1=0.9,\beta_2=0.95$
SCION	0.05	$\beta=0.5$
D-Muon	0.1	$\beta_1=0.9,\beta_2=0.95,\beta_3=0.95$
LANTON	0.1	$\beta_1=0.6,\beta_2=0.85$

E Comparison with Adaptive Variant of Muon

We additionally compared our method with the recently proposed adaptive variant AdaMuon (Si et al., 2025). Unlike LANTON, AdaMuon does not perform gradient noise estimation; instead, it introduces a momentum-style adaptive scaling on top of Muon and therefore is not noise-adaptive.

In our experiments, AdaMuon achieves slightly better performance than the original Muon but remains worse than LANTON. This matches our design motivation: LANTON is explicitly gradient noise-adaptive, adjusting each layer's learning rate based on its noise level. AdaMuon does not estimate noise and only plug a second-momentum term to Muon, providing limited gains.

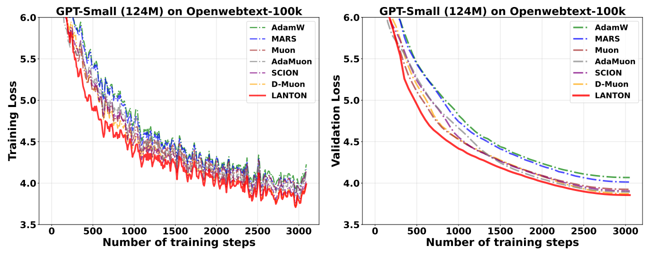

Figure 6: Training and validation loss on Openwebtext-100k.

F Noise Heterogeneity

F.1 Implementation Details of Figure 1

In this section, we provide implementation details of Figure 1. We pretrain LLaMA-1.1B model on C4 dataset for 10k steps, and apply momentum orthogonalized update to the matrix parameters $W_\ell \in \mathbb{R}^{d_{\text{out}} \times d_{\text{in}}}$ in the hidden layers (Query, Key, Value, MLP) and AdamW optimizer to the embedding and last layers. We first estimate gradient noise for two parameter groups, formed by matrix shape. For each weight matrix, we compute $\max(d_{\text{out}}, d_{\text{in}})$ and bucket it accordingly. We then aggregate the gradient-noise measure within each bucket over training (e.g., averaging across parameters in the group at each iteration) to obtain group-wise trajectories, which is shown in subfigure 1. Then we measure the layer-wise gradient noise within QK, VO, and MLP layer group in the last three subfigures.

The stochastic gradient noise is estimated by the nuclear norm (for parameters in Muon optimizer) or $\ell_1 \to \ell_1$ operator norm (for parameters in AdamW optimizer) of the difference between the current step's gradient and the previous step's gradient. The implementation follows Option I of line 7 in Algorithm 1 and line 4 in Table 1.

F.2 Noise Magnitude across Different Layer Groups

We estimate the layer-wise gradient noise within the QK, VO, and MLP layer groups at the midpoint of training (5,000 steps). We find large layer-to-layer disparities within each group, indicating that gradient noise is far from uniform within a group. The statistics is presented in Table 3.

Table 3: The statistics of stochastic gradient noise in different layer groups of LLaMA.

Layer Group	**#Layers**	$\bar{\sigma}$	$\underline{\sigma}$	σ_{mean}
QK	44	0.026	0.003	0.014
VO	44	0.117	0.009	0.046
MLP	66	0.107	0.018	0.038

G Model Configurations

We pretrain two types of model, GPT2 and LLaMA, the model configurations are listed in Table 4.

Table 4: Model configurations (d_{model} denotes the hidden dimension, d_{FF} denotes the feed-forward dimension, and n_{head} denotes the number of attention head in transformer).

Model	**Size**	d_{model}	d_{FF}	n_{head}	**depth**
GPT-2 (small)	124M	768	3072	12	12
GPT-2 (medium)	355M	1024	4096	16	24
LLaMA (0.5B)	522M	1280	5120	20	15
LLaMA (1.1B)	1175M	2048	5632	32	22

H Hyperparameter Settings

H.1 Hyperparameter Settings in GPT2 Experiments

We tune the base learning rate $\eta_{\max}$ for each method via a grid search in the range of $[1 \times 10^{-4}, 5 \times 10^{-3}]$. For Muon baseline, we additionally sweep a separate base learning rate for non-hidden (embedding/output) layers. All runs use cosine decay from $\eta_{\max}$ down to $\eta_{\min} = 0.0$. Muon and D-Muon use three momentum hyperparameters: (β_1, β_2) for the AdamW auxiliary optimizer and β_3 for orthogonalized momentum updates. LANTON uses two momentum parameters: β_1 for the gradient momentum and β_2 for the gradient noise momentum. All LMO-based methods (SCION, D-Muon, LANTON) apply layer-group learning-rate scaling; for SCION and D-Muon we adopt the best tuned scales reported in their original papers. All the hyperparameter settings are summarized in Table 5 and 6.

Table 5: The hyperparameter settings in GPT2-Small experiments.

Method	$\eta_{\max}$	Moment	Scale
AdamW	1×10^{-4}	$\beta_1 = 0.9, \beta_2 = 0.95$	-
Muon	$(3 \times 10^{-3}, 3 \times 10^{-4})$	$\beta_1 = 0.9, \beta_2 = 0.95, \beta_3 = 0.95$	-
MARS	1×10^{-3}	$\beta_1 = 0.9, \beta_2 = 0.95$	-
SCION	3×10^{-4}	$\beta = 0.9$	$r_1 = 50, r_2 = 3000$
D-Muon	1×10^{-3}	$\beta_1 = 0.9, \beta_2 = 0.95, \beta_3 = 0.95$	$r = 0.2$
LANTON	5×10^{-3}	$\beta_1 = 0.95, \beta_2 = 0.9$	$r_1 = 300, r_2 = 1.0$

Table 6: The hyperparameter settings in GPT2-Medium experiments.

Method	$\eta_{\max}$	Moment	Scale
AdamW	1×10^{-4}	$\beta_1 = 0.9, \beta_2 = 0.95$	-
Muon	$(3 \times 10^{-3}, 3 \times 10^{-4})$	$\beta_1 = 0.9, \beta_2 = 0.95, \beta_3 = 0.95$	-
MARS	1×10^{-3}	$\beta_1 = 0.9, \beta_2 = 0.95$	-
SCION	2×10^{-4}	$\beta = 0.9$	$r_1 = 50, r_2 = 3000$
D-Muon	5×10^{-4}	$\beta_1 = 0.9, \beta_2 = 0.95, \beta_3 = 0.95$	$r = 0.2$
LANTON	3×10^{-3}	$\beta_1 = 0.95, \beta_2 = 0.9$	$r_1 = 300, r_2 = 1.0$

H.2 Hyperparameter Settings in LLaMA Experiments

The best base learning rate for each algorithm is grid searched over $\{1 \times 10^{-4}, 3 \times 10^{-4}, 5 \times 10^{-4}, 1 \times 10^{-3}, 3 \times 10^{-3}, 5 \times 10^{-3}\}$. The decayed layer rate is set as $\eta_{\min} = 1/10\eta_{\max}$ on C4 and $\eta_{\min} = 1/20\eta_{\max}$ on Minipile. We keep the momentum and scale parameters as that in GPT2 experiments. The hyperparameter choices on C4 and Minipile are summarized in Tables 7 and 8, respectively.

Table 7: The hyperparameter settings on C4.

Method	$\eta_{\max}$	$\eta_{\min}$	Moment	Scale
AdamW	3×10^{-4}	3×10^{-5}	$\beta_1 = 0.9, \beta_2 = 0.95$	-
Muon	$(5 \times 10^{-3}, 3 \times 10^{-4})$	$(5 \times 10^{-4}, 3 \times 10^{-5})$	$\beta_1 = 0.9, \beta_2 = 0.95, \beta_3 = 0.95$	-
MARS	1×10^{-3}	1×10^{-4}	$\beta_1 = 0.9, \beta_2 = 0.95$	-
SCION	5×10^{-4}	5×10^{-5}	$\beta = 0.9$	$r_1 = 50, r_2 = 3000$
D-Muon	5×10^{-3}	5×10^{-4}	$\beta_1 = 0.9, \beta_2 = 0.95, \beta_3 = 0.95$	$r = 0.2$
LANTON	5×10^{-3}	5×10^{-4}	$\beta_1 = 0.95, \beta_2 = 0.9$	$r_1 = 300, r_2 = 1.0$

Table 8: The hyperparameter settings on Minipile.

Method	$\eta_{\max}$	$\eta_{\min}$	Moment	Scale
AdamW	8×10^{-4}	4×10^{-5}	$\beta_1 = 0.9, \beta_2 = 0.95$	-
Muon	$(5 \times 10^{-3}, 5 \times 10^{-4})$	$(2.5 \times 10^{-4}, 2.5 \times 10^{-5})$	$\beta_1 = 0.9, \beta_2 = 0.95, \beta_3 = 0.95$	-
MARS	1×10^{-3}	5×10^{-5}	$\beta_1 = 0.9, \beta_2 = 0.95$	-
SCION	5×10^{-4}	2.5×10^{-5}	$\beta = 0.9$	$r_1 = 50, r_2 = 3000$
D-Muon	5×10^{-3}	2.5×10^{-4}	$\beta_1 = 0.9, \beta_2 = 0.95, \beta_3 = 0.95$	$r = 0.2$
LANTON	5×10^{-3}	2.5×10^{-4}	$\beta_1 = 0.95, \beta_2 = 0.9$	$r_1 = 300, r_2 = 1.0$

I ROBUSTNESS

The training and validation loss curves with different base learning rates are presented in Figure 7.

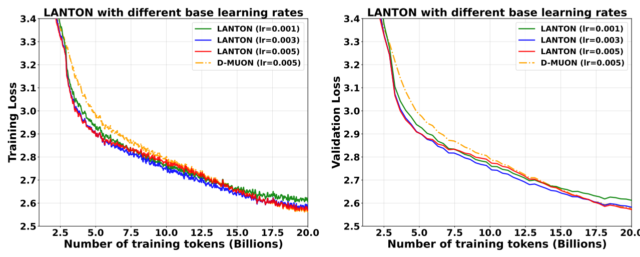

Figure 7: LANTON is robust to the choices of base learning rates.

J RUNNING TIME

To efficiently estimate the nuclear norm term $\|G_t^\ell - \tilde{G}_t^\ell\|_*^2$ for hidden-layer gradients (QK, VO, and MLP layers), we adopt the randomized singular value decomposition (R-SVD) method (Halko et al., 2011; Oh et al., 2015). The nuclear norm of a matrix is defined as the sum of its singular values, i.e., $\|A\|_* = \sum_i \sigma_i(A)$, where $\sigma_i(A)$ denotes the i-th singular value. Instead of computing a full SVD, we project $A = G_t^\ell - \tilde{G}_t^\ell$ onto a randomly generated low-dimensional subspace (with empirical dimension $d = 100$) and perform a small SVD on this reduced matrix to estimate its leading singular values. This approximation strategy is also used in SCION Pethick et al. (2025) in their implementation `https://github.com/LIONS-EPFL/scion/blob/main/examples/airbench/airbench_muon.py#L163`. The detailed implementation is provided in lines 44–70 of the submitted code file `train_llama/lanton.py`.

To further reduce computational cost, the gradient-noise estimation step (line 7 in Algorithm 1) is executed once every 10 iterations. We benchmark the runtime over 10 steps against other baselines, and the average computation time of each method is summarized in Table 9. Compared with the state-of-the-art baseline D-Muon, LANTON requires roughly 3 additional seconds per 10 iterations for gradient-noise estimation, resulting in an extra 0.84 hours of total training time. This corresponds to an overhead of only about 4% relative to D-Muon. Moreover, Figure 8(a) reports the wall-clock runtime comparison. As shown, LANTON achieves a noticeably faster early loss decrease and then maintains a trajectory comparable to D-Muon for the remainder of training. These results demonstrate that our method introduces only negligible computational overhead and achieves runtime on par with the SOTA baseline.

Table 9: The comparison of running time.

Method	Time (second)/10 steps	Total running time (hours)
AdamW	64.55	18.53
Muon	69.62	19.96
MARS	69.01	19.78
SCION	71.53	20.49
D-Muon	70.07	20.08
LANTON	73.08	20.92

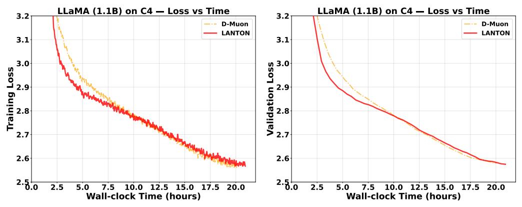

(a) Running time on 1.1B model.

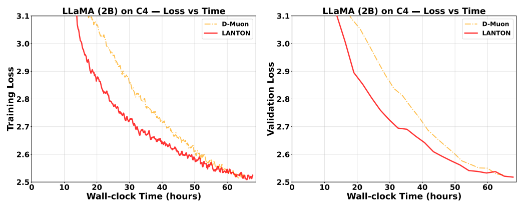

(b) Running time on 2B model.

Figure 8: Training and validation loss vs. wall-clock time.

K Evolution of Effective Learning Rate

The early-stage speedup arises because gradient noise varies significantly across layers at the beginning of training. As shown in Figure 9, the hidden layers (in subfigure (a)) start with an averaged effective learning-rate mean of 0.0028 and a standard deviation of 0.0007, indicating notable layerwise differences that LANTON can exploit to accelerate optimization in the early stage. By the end of training, cosine decay drives all learning rates toward very small values, and the hidden-layer learning rates converge to a mean of 0.00016 with a much smaller standard deviation of 0.00008. The reduced variance shows that layerwise learning rates become nearly uniform in the later stage of the training, and therefore layerwise learning rate is equivalent to using the same learning rate in the same group and the benefit diminishes.

Importantly, LANTON achieves faster early loss descent while still reaching comparable or better final performance, demonstrating that its advantage to accelerate training with noise-adaptive layerwise learning rates.

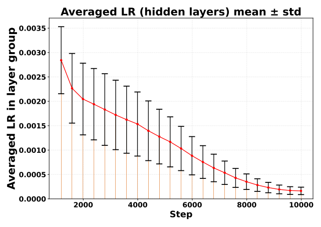

(a)

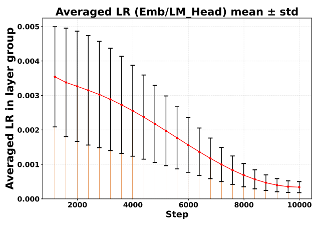

(b)

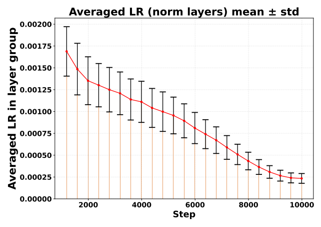

(c)

Figure 9: The statistics of learning rate in 3 layer groups: (a) start: 0.0028 ± 0.0007, end: 0.00016 ± 0.00008; (b) start: 0.0035 ± 0.0015, end: 0.00034 ± 0.00016; (c) start: 0.0017 ± 0.0003, end: 0.0002 ± 0.00006.

L Ablation of Batch Size

To assess the influence of batch size on stochastic gradient variance estimation, we trained GPT (124M) models on openwebtext-100k with batch sizes BS $= \{8, 16, 32, 48, 64\}$ for one epoch (the number of training tokens is fixed to 46 million). For each batch size, we independently tuned the learning rate to its best-performing values (1.0×10^{-2} for BS=8, 5.0×10^{-3} for other BS settings), ensuring a fair comparison across different settings. As shown in training loss curve in Figure 10, smaller batches yield noisier trajectories while larger batches produce smoother curves, yet all settings converge to nearly the same final training and validation loss (approximately 4.0).

These results demonstrate that our method is highly robust to batch-size variation: the convergence behavior and final performance are reasonably good and consistent across a wide range of batch sizes. Among the configurations, BS $= 16$ provides the best model performance, which is used in the main experimental settings.

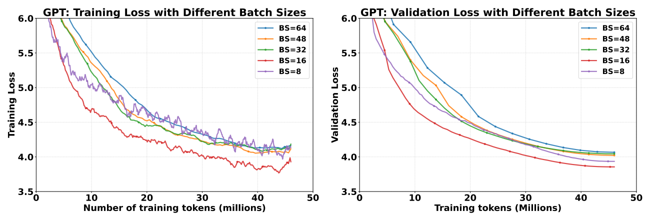

Figure 10: Training and validation loss vs. batch sizes (BS).

M Gradient Noise Estimation: Option I vs. Option II

We compared the performance of Options 1 and 2 in Algorithm 1. As described in line 7, our main experiments use Option 2 with GPT-124M on Openwebtext-100k. For Option 1, estimating gradient noise requires two independent mini-batches per iteration; therefore, under a fixed one-epoch budget, Option 1 performs only half as many optimization steps as Option 2.

Figure 11 reports the training and validation curves for both settings. With the same one-epoch budget, Option 1 achieves much lower final training and validation loss than Option 2 because it performs more gradient updates.

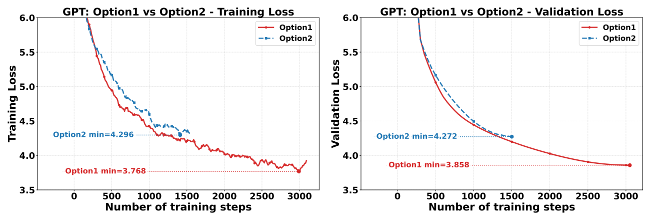

Figure 11: Training and validation loss with two gradient noise estimation options.

N License of Models and Datasets

GPT2 OpenAI's GPT2 models are distributed by MIT License. We use only the open-source implementation of the GPT2 architecture in Hugging Face Transformers and do not redistribute Meta's model weights.

LLaMA We follow Meta Llama 2 Community License Agreement. We use only the open-source implementation of the LLaMA architecture in Hugging Face Transformers and do not redistribute Meta's model weights.

C4 The English portion of the C4 (Colossal Clean Crawled Corpus) dataset comes from Hugging Face (allenai/c4), which is distributed under the Open Data Commons Attribution (ODC-By 1.0) license.

Minipile It can be accessed from Hugging Face (JeanKaddour/minipile), which is distributed under MIT License.

Openwebtext It can be accessed from Hugging Face (Skylion007/openwebtext), which is distributed under Creative Commons cc0-1.0 license.

O The Use of Large Language Models (LLMs)

LLMs are not involved in our research methodology. Their use is limited to polish the writing.